

1 **Carm1 regulates the speed of C/EBP α -induced transdifferentiation by a cofactor stealing**
2 **mechanism**

3

4 Guillem Torcal Garcia^{1,2*}, Elisabeth Kowenz-Leutz^{3*}, Tian V. Tian^{1,2,4*}, Antonios Klonizakis^{1,2},
5 Jonathan Lerner⁵, Luisa de Andrés-Aguayo^{1,2}, Clara Berenguer^{1,2}, Marcos Plana-Carmona^{1,2},
6 Maria Vila-Casadesús^{1,2,4}, Romain Bulteau⁶, Mirko Francesconi⁶, Sandra Peiró⁴, Kenneth S.
7 Zaret⁵, Achim Leutz^{3,7#}, Thomas Graf^{1,2#}

8 ¹Gene Regulation, Stem Cells and Cancer Program, Centre for Genomic Regulation (CRG), The
9 Barcelona Institute of Science and Technology (BIST), Carrer del Doctor Aiguader 88, 08003
10 Barcelona, Spain

11 ²Universitat Pompeu Fabra (UPF), Carrer del Doctor Aiguader 88, 08003 Barcelona, Spain.

12 ³Max Delbrück Center for Molecular Medicine in the Helmholtz Association, Robert-Rössle-
13 Strasse 10, 13125 Berlin, Germany.

14 ⁴Vall d'Hebron Institute of Oncology (VHIO), Carrer de Natzaret 115-117, 08035 Barcelona,
15 Spain.

16 ⁵Institute for Regenerative Medicine and Department of Cell and Developmental Biology,
17 Perelman School of Medicine, University of Pennsylvania, 3400 Civic Center Blvd, PA 19104
18 Philadelphia, USA.

19 ⁶Laboratoire de Biologie et Modélisation de la Cellule, Université de Lyon, ENS, UCBL, CNRS,
20 INSERM, UMR5239, U 1210, F-69364 Lyon, France.

21 ⁷Institute of Biology, Humboldt University of Berlin, Invalidenstrasse 42, 10115 Berlin, Germany.

22 *,#Equal contributions

23 Correspondence: thomas.graf@crg.eu; aleutz@mdc-berlin.de

24 **ABSTRACT**

25 Cell fate decisions are driven by lineage-restricted transcription factors but how they are
26 regulated is incompletely understood. The C/EBP α -induced B cell to macrophage
27 transdifferentiation (BMT) is a powerful system to address this question. Here we describe that
28 C/EBP α with a single arginine mutation (C/EBP α ^{R35A}) induces a dramatically accelerated BMT
29 in mouse and human cells. Changes in the expression of lineage-restricted genes occur as early
30 as within 1 hour compared to 18 hours with the wild type. Mechanistically C/EBP α ^{R35A} exhibits
31 an increased affinity for PU.1, a bi-lineage transcription factor required for C/EBP α -induced BMT.
32 The complex induces more rapid chromatin accessibility changes and an enhanced relocation
33 (stealing) of PU.1 from B cell to myeloid gene regulatory elements. Arginine 35 is methylated by
34 Carn1 and inhibition of the enzyme accelerates BMT, similar to the mutant. Our data suggest
35 that the relative proportions of methylated and unmethylated C/EBP α in bipotent progenitors
36 determine the velocity of cell fate choice and also affect lineage directionality. The PU.1 stealing
37 mechanism described can explain how the faithfulness of a cell fate conversion is maintained
38 even when its velocity varies.

39

40 INTRODUCTION

41 The hematopoietic system is a model of choice to understand how cells diversify into different
42 lineages (Notta et al., 2016; Orkin and Zon, 2008). Combinations of synergistic and antagonistic
43 transcription factors (TFs) are the main drivers of cell fate decisions, activating new gene
44 expression programs while silencing the old ones. Their balance is an important determinant,
45 with the most highly expressed factors becoming dominant (Graf and Enver, 2009; Okawa et al.,
46 2018; Orkin and Zon, 2008). However, whether there are other determinants that modulate the
47 factors' activity and thus the velocity by which a precursor chooses alternative fates remains
48 poorly understood.

49 A powerful approach to study the mechanism of cell fate decisions is TF-induced lineage
50 conversions (Graf and Enver, 2009). C/EBP α induces the efficient transdifferentiation of B and T
51 lineage cells into monocyte/macrophages (henceforth referred as macrophages) (Laiosa et al.,
52 2006; Xie et al., 2004). This conversion requires the transcription factor PU.1, a key component
53 of the regulatory networks that define lymphoid and myeloid cells (Arinobu et al., 2007; Leddin et
54 al., 2011; Singh et al., 1999). C/EBP α contains a C-terminal basic region leucine zipper DNA-
55 binding domain (bZip) as well as an N-terminal transactivation domain divided into distinct
56 transactivating elements (TE-I, II and III) (Ramberger et al., 2021). During hematopoiesis it is
57 most highly expressed in granulocyte-macrophage progenitors (GMPs) (Ohlsson et al., 2016)
58 and its ablation blocks the formation of GMPs and granulocytes while reducing the number of
59 monocytes (Heath et al., 2004; Ma et al., 2014; Zhang et al., 2004).

60 Protein post-translational modifications can alter protein structure, subcellular localization and
61 interactome and may dynamically coordinate signaling networks (Deribe et al., 2010; Torcal
62 Garcia and Graf, 2021). Arginine methylation is a common protein modification effected by
63 protein arginine methyltransferases (Prmts), which can catalyze asymmetrical and symmetrical
64 arginine dimethylation, as well as monomethylation (Wu et al., 2021). While most studies on the
65 role of arginine methylation have focused on histones it may also affect the function of proteins
66 involved in DNA replication (Guo et al., 2010) and differentiation (Kawabe et al., 2012; Kowenz-
67 Leutz et al., 2010). Among the Prmts, Carm1 (Prmt4) is particularly relevant for developmental
68 decisions such as during early embryo development, adipogenesis and muscle regeneration, as

69 well as for cancer (Kawabe et al., 2012; Kim et al., 2010; Li et al., 2013; M. E. Torres-Padilla et
70 al., 2007; Yadav et al., 2008).

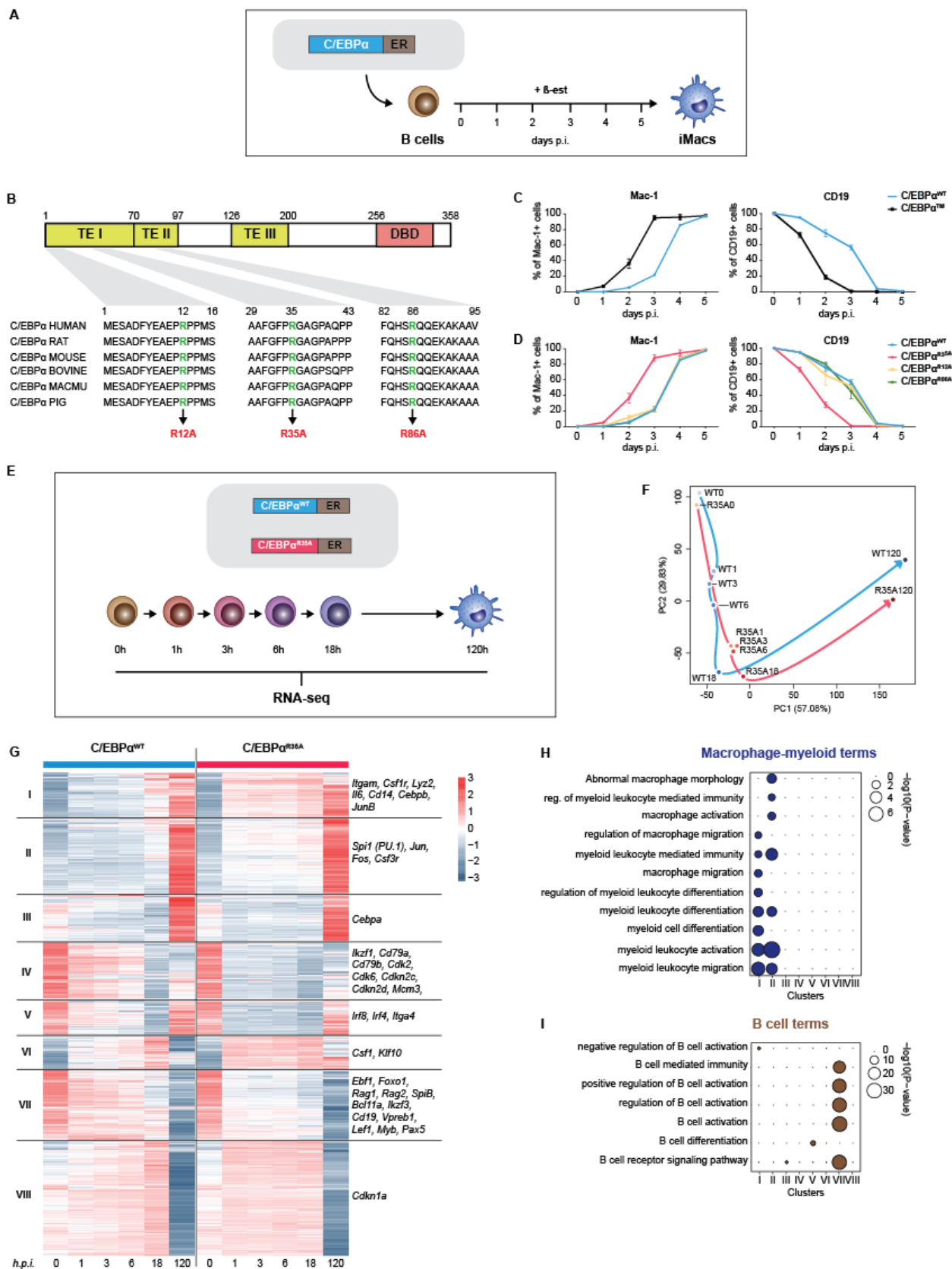
71 Here we describe that the methylation of a specific arginine within the transcription
72 activation domain of C/EBP α by the arginine methyltransferase Carm1 dampens the speed by
73 which the factor induces transdifferentiation. Mechanistically, the unmethylated form of C/EBP α
74 accelerates BMT induction by the enhanced relocation ('stealing') of its partner PU.1 from B cell
75 gene regulatory regions to myeloid regions, accompanied by an accelerated closing and opening
76 of chromatin. Our data suggest that the two forms of C/EBP α bias the differentiation of bipotent
77 progenitors towards alternative lineages.

78

79 RESULTS

80 Mutation of arginine 35 of C/EBP α accelerates immune cell transdifferentiation

81 To identify post-translational modifications that are associated with the BMT-inducing ability of
82 C/EBP α (**Figure 1A**), we focused on arginines in the factor's transactivation domain. We
83 identified three evolutionarily conserved arginines (R12, R35, and R86) located within the N-
84 terminus (**Figure 1B**) in two transactivating elements (TE-I and TE-II) required for efficient BM
85 (Stoilova et al., 2013). First we generated a triple mutant (C/EBP α TM) in which these arginines
86 were substituted by alanines (Figure 1B) and inserted it into a β -estradiol (β -est)-inducible
87 retroviral vector (Xie et al., 2004), generating C/EBP α TM-ER-GFP. This construct was used to
88 infect bone marrow-derived B cell precursors (henceforth called B cells) grown on feeder cells
89 for 2 days and GFP+ B cells isolated. The infected cells were re-seeded on feeders, cultures
90 treated with β -est and expression of the macrophage marker Mac-1 (CD11b) and the B cell
91 marker CD19 (Springer et al., 1979; Wang et al., 2012) monitored by FACS at various days later.
92 Surprisingly, C/EBP α TM greatly accelerated BMT, generating almost 100% macrophage-like cells
93 (Mac-1+, CD19-) within 3 days compared to 4 to 5 days for C/EBP α WT-infected cells (**Figure,**
94 **1C, S1A**).



96 **Figure 1. Mutation of arginine 35 in C/EBP α accelerates B cell to macrophage transdifferentiation. A.**
97 Schematics of the B cell to macrophage transdifferentiation (BMT) method. Bone marrow-derived pre-B cells
98 infected with C/EBP α -ER retrovirus are treated with β -est to induce the factor's translocation into the nucleus,
99 inducing a BMT within 4 to 5 days. **B.** C/EBP α structure (TE = transactivation element; DBD = DNA-binding domain)
100 and location of conserved arginines R12, R35, and R86 within the N-terminus, which were replaced by alanines. **C.**
101 Kinetics of BMT induced by wild type (WT) C/EBP α and a triple mutant (C/EBP α^{TM}) with alanine replacements of
102 R12, R35 and R86. BMT was assessed by Mac-1 and CD19 expression (mean \pm s.d., n=3). **D.** Kinetics of BMT
103 induced by C/EBP α^{WT} and single arginine to alanine replacements at C/EBP α R12, R35, and R86. **E.** Schematics
104 of experimental approach for RNA-sequencing (RNA-seq) of B cells infected with either C/EBP α^{WT} - or C/EBP α^{R35A} -
105 ER retroviral constructs induced for various timepoints. **F.** Principal component analysis (PCA) of 11,780
106 differentially expressed genes (DEGs) during BMT (n=2). Arrows connecting individual time points visualize
107 trajectories **G.** Hierarchical clustering of DEGs with representative genes shown next to each cluster. **H-I.** Gene
108 ontology (GO) enrichment analysis of macrophage-myeloid (**H**) and B cell (**I**) terms of the clusters from Figure 1G.
109 Diameter of circles is proportional to the p-value. See also **Figure S1**.

110 Next, we tested the effect of alanine replacement for each of the 3 individual arginines (R12A,
111 R35A, and R86A) and found that C/EBP α^{R35A} recapitulated the phenotype of C/EBP α^{TM} , while
112 C/EBP α^{R12A} and C/EBP α^{R86A} showed no such effect (**Figures 1D, S1A**). Five-day-induced
113 C/EBP α^{R35A} cells resembled normal macrophages similar to those seen with C/EBP α^{WT} cells,
114 consisting of large, mostly adherent cells, with extensive f-actin filaments and eccentric nuclei.
115 In addition, the cells were highly phagocytic, as >90% of them ingested carboxylated beads
116 (**Figures S1B, C**).

117 These data show that the replacement of arginine 35 with alanine in C/EBP α dramatically
118 accelerates the factor's capacity to induce a BMT, as evidenced by a higher velocity of silencing
119 and activation of B cell and macrophage markers, respectively. Moreover, the induced cells
120 resembled normal macrophages and were functional.

121 **C/EBP α^{R35A} hastens gene expression changes of lineage-associated genes at early time** 122 **points**

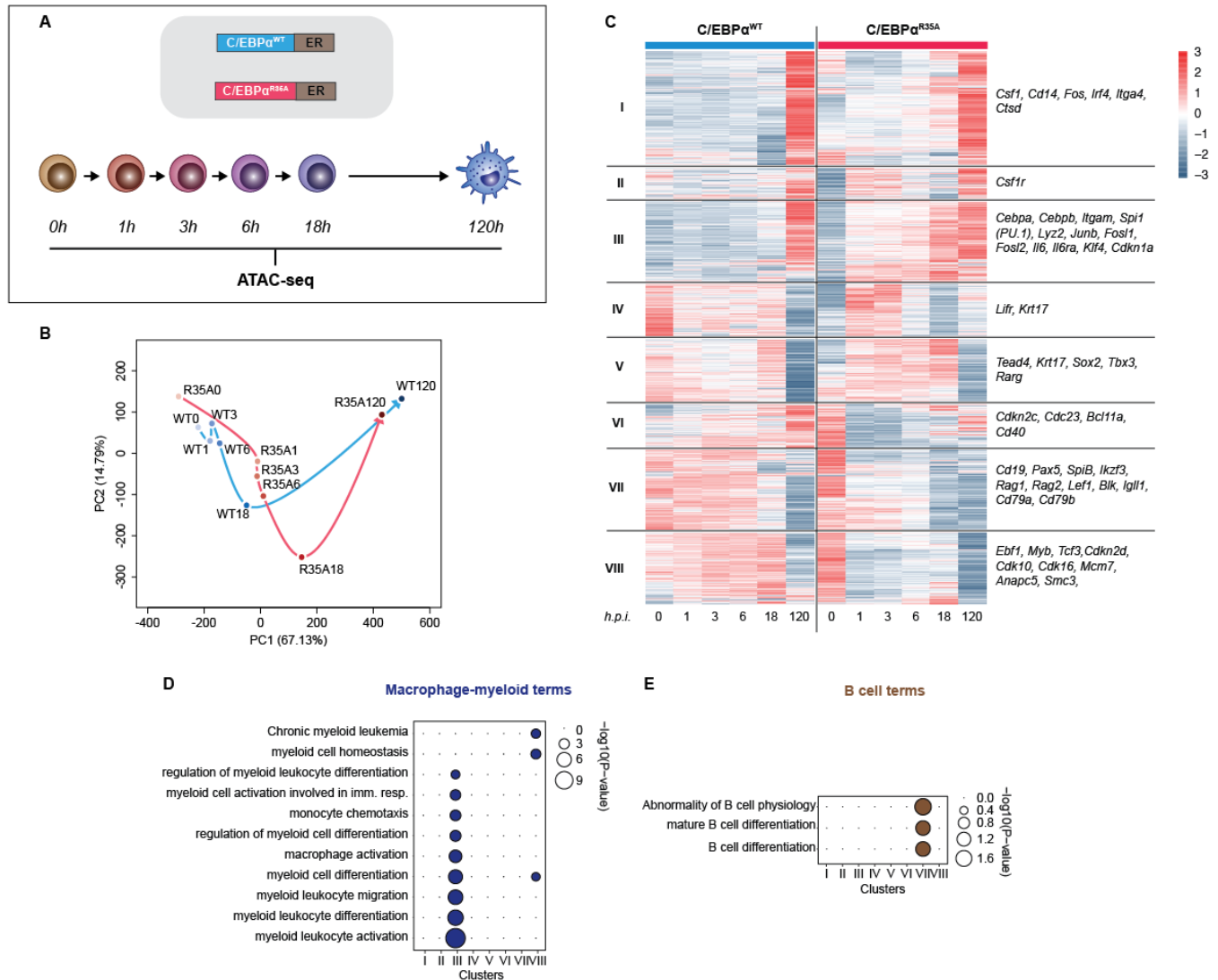
123 To study the effects of C/EBP α^{R35A} on gene expression, we performed RNA-sequencing
124 (RNA-seq) of infected B cells induced for 0, 1, 3, 6, 18, and 120 hours (**Figure 1E**). Principal
125 component analysis (PCA) showed a pronounced acceleration in the trajectory of differentially
126 expressed genes throughout BMT (11,780 genes) compared to the WT virus. Strikingly, induction
127 of C/EBP α^{R35A} cells for just 1 hour caused changes similar to 18 hours induced C/EBP α^{WT} cells,

128 with their trajectories converging again at 120 hours post induction (hpi; **Figure 1F**). The vast
129 majority of genes affected by the wild type and the mutant exhibited similar expression levels at
130 the endpoint of the conversion, indicating that the mutant mostly accelerates the speed of BMT
131 without inducing an aberrant phenotype (**Figure S1D**). Moreover, the largest differences in gene
132 expression values between wild type and mutant cells were observed at 1 and 3 hpi (**Figure**
133 **S1D**). Hierarchical clustering of all the 11,780 differentially expressed genes throughout BMT
134 yielded 8 clusters (**Figure 1G**). These could be separated into two large groups, with genes in
135 clusters I, II, IV and VIII displaying faster activation by C/EBP α ^{R35A}, while clusters IV, V and VII
136 showed faster silencing. Macrophage-myeloid related GO terms were enriched in clusters I and
137 II (**Figures 1H, S1F**) and included the myeloid-restricted genes *Irgam* (encoding Mac-1) *Lyz2*
138 (lysozyme), *Csf1r* (M-CSF receptor) and *Cd14* (**Figures 1G, S1G**). Conversely, B cell-related
139 GO terms were enriched in cluster VII (**Figures 1I, S1F**) and included the B cell-restricted genes
140 *Cd19*, *Pax5*, *Ebf1* and *Rag2* (**Figures 1G, S1G**). The kinetics of individual macrophage and B
141 cell-associated genes (**Figure S1H**) further illustrate the C/EBP α ^{R35A}-induced BMT acceleration.

142 These results extend the findings obtained with B cell and macrophage cell surface markers
143 to thousands of differentially regulated lineage-associated genes. The most dramatic differences
144 in gene expression changes induced by C/EBP α ^{R35A} occurred within 3 hpi and then converged
145 again at 120 hpi.

146 **C/EBP α ^{R35A} accelerates chromatin remodelling at regulatory elements of lineage-** 147 **restricted genes**

148 Major gene expression changes are typically associated with extensive chromatin remodeling
149 (Klemm et al., 2019). To study changes in chromatin accessibility occurring during BMT, we
150 performed assays for Transposase-Accessible Chromatin using sequencing (ATAC-seq) at
151 various time points after C/EBP α ^{WT} and C/EBP α ^{R35A} induction (**Figure 2A**).



152

153 **Figure 2. C/EBP α^{R35A} accelerates chromatin accessibility at gene regulatory elements of lineage-restricted**
 154 **genes. A.** Experimental approach used for chromatin accessibility profiling. B cells infected with either C/EBP α^{WT} -
 155 ER or C/EBP α^{R35A} -ER retroviral constructs (n=2 biological replicates) were induced for the indicated times and
 156 processed for ATAC-seq. **B.** PCA of differential chromatin accessibility dynamics during BMT induced by C/EBP α^{WT}
 157 (cyan) or C/EBP α^{R35A} (magenta), based on 91,830 ATAC-seq peaks differentially called for the two conditions.
 158 Arrows connecting individual timepoints show trajectories. **C.** Hierarchical clustering of differentially accessible
 159 promoters (14,233 peaks) with representative genes shown next to each cluster. **D-E.** Gene ontology analysis of
 160 macrophage-myeloid (**D**) and B cell (**E**) terms of each cluster. Diameter of circles is proportional to the p-value. See
 161 also **Figure S2**.

162 ATAC-seq revealed 91,830 peaks significantly different between wild type and mutant cells in at
 163 least one time point, indicating differential chromatin accessibility. These regions fell into three
 164 groups: a) faster opening Gene Regulatory Elements (GREs), with highest peaks at 120hpi

165 (43,429 peaks); b) faster closing GREs, with highest peaks at 0 hpi (36,380 peaks) and c)
166 transiently opening GREs with highest peaks at 18 hpi (12,021 peaks) (**Figure S2A, B**). While
167 both opening and closing GREs showed a largely accelerated trend with C/EBP α ^{R35A}, transiently
168 opening GREs showed only subtle differences between the two conditions (**Figure S2B**). PCA
169 analysis of the differential ATAC peaks revealed an acceleration of chromatin accessibility by
170 C/EBP α ^{R35A} (**Figure 2B**), with values of the 1-6 hpi C/EBP α ^{R35A} samples resembling the 18 hpi
171 C/EBP α ^{WT} sample.

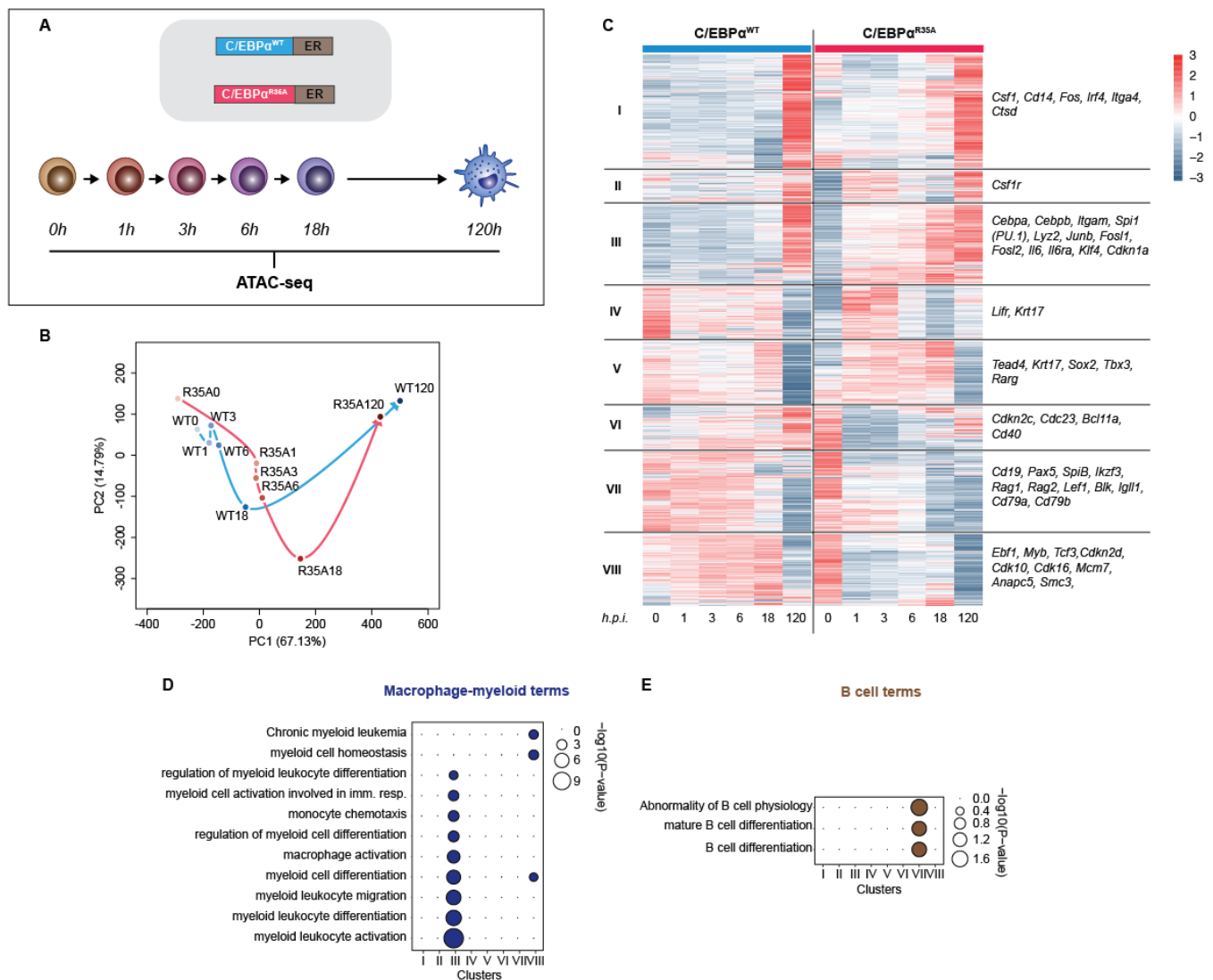
172 We then grouped the 14,233 differential peaks at promoter regions into eight clusters, with
173 genes in clusters I, II and III exhibiting opening dynamics dramatically accelerated by
174 C/EBP α ^{R35A}, while genes in clusters VII and VIII showing accelerated closing (**Figure 2C**). GO
175 analysis revealed an enrichment of macrophage terms for cluster III (**Figure 2D**) and included
176 the macrophage-restricted genes *Itgam* and *Lyz2* (**Figure 2C**). Quantification of accessibility
177 changes in GREs (including promoters and enhancers of genes) in this cluster showed an
178 accelerated chromatin opening by C/EBP α ^{R35A} at the early timepoints (exemplified by *Itgam* and
179 *Lyz2* in **Figure S2C**). Conversely, the faster closing GREs in cluster VIII were enriched for B cell-
180 related GO terms and included the B cell genes *Cd19*, *Pax5* and *Rag2* (**Figures 2C, E, S2D**).
181 Differences in chromatin accessibility at these clusters were no longer apparent at 120 hpi
182 (**Figures 2B, C**).

183 Overall, these results indicate that C/EBP α ^{R35A} is more efficient at inducing chromatin opening
184 or closing at lineage-specific GREs compared to C/EBP α ^{WT}, consistent with the observed
185 acceleration of gene expression changes (**Figure 1E-I**). Again, these differences are most
186 pronounced at the earliest time points.

187 **Differentially opening and closing chromatin regions are enriched for PU.1 motif**

188 To test whether the accelerated changes in chromatin accessibility are due to differential DNA
189 binding affinities, we performed an electrophoretic mobility shift assay with both proteins, using
190 nuclear extracts from HEK-293T cells expressing either C/EBP α ^{WT} or C/EBP α ^{R35A}. These were
191 incubated with an end-labeled oligonucleotide containing a palindromic C/EBP α -binding motif
192 and run on an a native acrylamide gel. The intensity of the resulting bands corresponding to

193 C/EBP α ^{WT} and C/EBP α ^{R35A} complexes were similar, indicating that the mutation does not
 194 significantly affect the DNA-binding capacity of the factor (**Figure 3A**).



195

196 **Figure 3. C/EBP α ^{R35A} exhibits an increased affinity for PU.1.** **A.** Electrophoretic mobility shift assay with nuclear
 197 extracts of HEK-293T cells transfected with either C/EBP α ^{WT} or C/EBP α ^{R35A} incubated with a fluorophore-labeled
 198 oligonucleotide containing a palindromic C/EBP α -binding motif (left). Protein expression control of nuclear C/EBP α
 199 proteins by western blot (middle) and densitogram-based relative DNA binding versus protein expression (right). **B.**
 200 Lists of the top *de novo* motifs in faster opening or closing GREs induced by C/EBP α ^{R35A} (**Figures S2A, B**), with the
 201 PU.1 motif indicated in red. Dashed lines correspond to the significance threshold of Q-value (≤ 0.05). **C.** Co-
 202 immunoprecipitation of PU.1 and C/EBP α in HEK-293T cells transfected with either C/EBP α ^{WT} or C/EBP α ^{R35A} (left)
 203 and quantification of interaction of three independent experiments (right). Values shown were normalized to the
 204 expression of C/EBP α (mean + individual values). Dashed lines indicate paired values; statistical significance was
 205 determined using a paired Student's t-test. **D.** Proximity ligation assay of C/EBP α and PU.1 in mouse B cells induced

206 with either C/EBP α ^{WT} or C/EBP α ^{R35A} for 24 hours. On the left, confocal microscopy images of the cells showing
207 nuclear dots. On the right, quantification of interactions by counting nuclear dots per cell (mean \pm s.e., n=30-34;
208 statistical significance determined using an unpaired Student's t-test). See also **Figure S3**.

209 Another possibility is that the altered chromatin remodeling capacity of C/EBP α ^{R35A} is due to
210 the differential interaction with another protein(s). In an attempt to find such potential interactors,
211 we performed a *de novo* motif discovery analysis with the differentially accessible GREs in the
212 three groups by matching them against known TF motifs (**Figure S2A and B**). Faster and
213 transiently opening GREs were found to be strongly enriched for AP-1/leucine zipper family TF
214 motifs (c-Fos, c-Jun and JunB), a family of factors known to be able to heterodimerize with
215 C/EBP α to activate myeloid genes (Cai et al., 2008). In contrast, faster closing GREs were mostly
216 enriched for ETS family TF motifs such as Ets1, Fli1, SpiB and Gabpa, known to be associated
217 with B cell lineage differentiation and function (Eyquem et al., 2004; Hu et al., 2001; Xue et al.,
218 2007; Zhang et al., 2008). Several motifs were also enriched in both the accelerated chromatin
219 opening and closing groups, including that of PU.1 and the closely related factor Spi-B (**Figures**
220 **3B, S3A**). Conversely, the transiently opening regions were enriched for AP-1 motifs but not for
221 PU.1 (**Figure S3B**).

222 These observations show that chromatin regions more rapidly opened by C/EBP α ^{R35A} are
223 enriched for AP-1 family binding motifs in line with the synergism between C/EBP α and AP-1
224 family factors during myeloid differentiation (Cai et al., 2008). Conversely, the association of Ets
225 family motifs with more rapidly closed regions might reflect the role of Fli1, Spi-B and in B cell
226 differentiation (Zhang et al., 2008). That the PU.1 motif is shared between faster opening and
227 closing regions might reflect its dual roles in the two lineages (Scott et al., 1994; Singh et al.,
228 1999).

229 **C/EBP α ^{R35A} exhibits an increased affinity for PU.1**

230 Since PU.1 is a necessary partner of C/EBP α during myeloid cell specification (Heinz et al., 2010;
231 van Oevelen et al., 2015; Xie et al., 2004) in the following we focused on the role of PU.1 during
232 BMT. To test whether arginine 35 modulates the interaction of C/EBP α with PU.1, we performed
233 co-immunoprecipitation experiments with cellular extracts from HEK293-T cells co-transfected
234 with PU.1 and either WT or mutant C/EBP α . This revealed an approximately 2-fold increase in
235 the interaction between C/EBP α ^{R35A} and PU.1 compared to C/EBP α ^{WT} (**Figure 3C**). Also,

236 proximity ligation assays showed a stronger interaction between PU.1 and C/EBP α ^{R35A}
237 compared to C/EBP α ^{WT}, as determined by a significantly higher number of fluorescent nuclear
238 dots (**Figure 3D**). These results therefore indicate that a mutation of C/EBP α ^{R35} increases the
239 factor's affinity for its obligate partner PU.1.

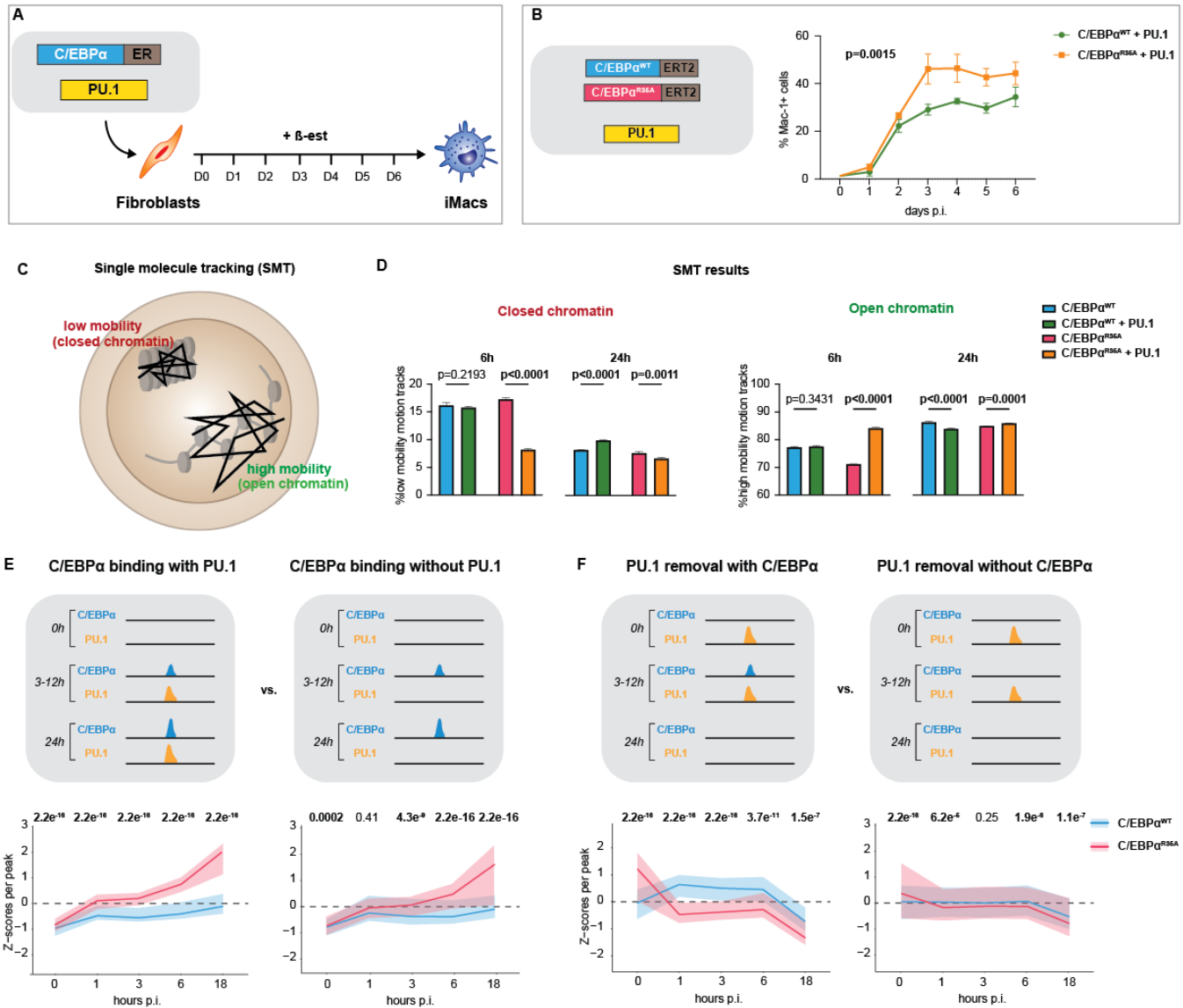
240 **C/EBP α ^{R35A} shows an increased synergy with PU.1 in fibroblasts**

241 We have previously shown that C/EBP α synergizes with PU.1 in converting NIH 3T3 fibroblasts
242 into macrophage-like cells (Feng et al., 2008a) (**Figure 4A**). Therefore, to determine how the
243 mutant behaves in this system, we generated NIH 3T3-derived cell lines (3T3aER-R and
244 3T3aER-A) stably expressing inducible forms of C/EBP α ^{WT} or C/EBP α ^{R35A}, respectively. These
245 lines were then infected with a constitutive PU.1 retroviral construct, treated with β -est, and Mac-
246 1 levels monitored by FACS at various times post-induction. As described earlier (Feng et al.,
247 2008b), the combination of C/EBP α ^{WT} with PU.1 activated Mac-1 expression while the individual
248 constructs did not (**Figures 4B, S4A, B**). Importantly, C/EBP α ^{R35A} synergized with PU.1 more
249 strongly than C/EBP α ^{WT} in activating Mac-1 (**Figures 4B, S4A**). In addition, cells co-expressing
250 PU.1 and C/EBP α ^{R35A} exhibited dramatic morphological changes, with cells co-expressing PU.1
251 and C/EBP α ^{WT} displaying more subtle alterations (**Figure S4C**).

252 **Single-molecule tracking experiments in fibroblasts show a PU.1-enhanced chromatin** 253 **opening by C/EBP α ^{R35A}**

254 To explore whether also in fibroblasts the two forms of C/EBP α exhibit differences in
255 chromatin opening and how this is influenced by PU.1, we performed single-molecule tracking
256 (SMT) experiments. This allows to visualize the Brownian-like movement of individual TF
257 molecules and their interaction with open and closed chromatin (Lerner et al., 2020; Liu and
258 Tjian, 2018) (**Figure 4C**). For this purpose, we generated NIH3T3 cells expressing doxycycline-
259 inducible Halo-tagged histone H2B, C/EBP α ^{WT} or C/EBP α ^{R35A}. After induction for either 6h or 24h
260 these cells were used to perform SMT on ~50 cells per condition and 20,000 single-molecule
261 motion tracks were randomly down-sampled in triplicates to compare each condition (Chen et
262 al., 2014). Monitoring the radius of confinement and average displacement of histone H2B
263 allowed us to define low and high mobility chromatin, corresponding to closed and open states,
264 respectively (Lerner et al., 2020) (**Figure S4D**).

265 Similar two-parameter assessment of motion tracks of C/EBP α ^{WT} and C/EBP α ^{R35A} showed
266 that after 6 hpi, both TFs display interactions with low mobility (closed) chromatin, with
267 C/EBP α ^{R35A} showing a slightly increased interaction (**Figure 4D**). This observation is consistent
268 with the elevated affinity for nucleosomes of C/EBP α measured *in vitro* (Fernandez Garcia et al.,
269 2019; Lerner et al., 2020). At 24 hpi, both C/EBP α ^{WT} and C/EBP α ^{R35A} showed a decreased
270 interaction with low mobility chromatin and increased interaction with high mobility chromatin
271 (**Figure 4D**). This transition to higher mobility chromatin suggests an opening of regions bound
272 by C/EBP α , consistent with the known pioneering function of C/EBP α (Fernandez Garcia et al.,
273 2019).



274

275

276

277

278

279

280

281

282

283

284

285

Figure 4. C/EBP α ^{R35A} shows an enhanced synergy with PU.1 and hastens its relocation from B cell to myeloid GRES. **A.** Schematic representation of TF-induced fibroblast to macrophage transdifferentiation. NIH3T3 fibroblasts were infected C/EBP α ^{WT}-ER or C/EBP α ^{R35A}-ER in the presence or absence of PU.1 construct. Cells were induced with β -est for the indicated times, causing a conversion to macrophage-like cells (iMacs) within 6 days p.i. **B.** Kinetics of Mac-1 expression (mean \pm s.d., n=3; statistical significance was determined using two-way ANOVA). **C.** Schematic representation of single molecule movements of TFs bound to closed (low mobility) or open (high mobility) chromatin. **D.** Quantification of single cell motion tracks (mean \pm s.d., n=3 x 20,000 randomized down sampled motion tracks; statistical significance determined using two-way ANOVA with multiple comparisons). **E, F.** Virtual chromatin immunoprecipitation of C/EBP α and PU.1 during BMT induced either by C/EBP α ^{WT} or C/EBP α ^{R35A} for the indicated times, showing schematics of peaks illustrating the different conditions tested. **E,** Selected regions corresponding to sites that are devoid of C/EBP α and PU.1 in B cells and become bound by both factors (left) or

286 only by C/EBP α (right) throughout BMT. **F** Selected regions corresponding to sites where PU.1 is bound in B cells
287 and either removed by transient binding of C/EBP α (left) or by another mechanism during BMT (right). See also
288 **Figure S4**. Data were computed from ATAC-seq experiments (**Figure 2**) and from ChIP-seq of C/EBP α and PU.1
289 in B cells induced with β -est for 0, 3, 12 and 24 hours (van Oevelen et al., 2015). Plots on the bottom show chromatin
290 accessibility Z-scores per ATAC peak of B cells induced with either wild type (cyan) or mutant C/EBP α (magenta)
291 at different hpi (line=median; shaded background=IQR; statistical significance was determined using a Wilcoxon
292 signed-rank test).

293 We then tested the effect of PU.1 co-expression on interactions of C/EBP α with open or
294 closed chromatin. At 6 hpi C/EBP α ^{R35A} cells co-expressing PU.1 displayed a dramatic decrease
295 in interaction with low mobility chromatin concomitantly with increased interaction with higher
296 mobility chromatin, while PU.1 co-expression had little effect on the mobility of C/EBP α ^{WT}. This
297 suggests a faster chromatin opening by C/EBP α ^{R35A} at sites bound by PU.1 (**Figure 4D** and **F**).
298 The observed differences between C/EBP α ^{WT} and C/EBP α ^{R35A} co-expressing PU.1 essentially
299 disappeared after 24h, suggesting that the two protein complexes open closed chromatin at
300 different speeds but reach similar endpoints (**Figure 4D** and **E**).

301 Altogether these results show that in 3T3 cells C/EBP α ^{R35A} displays an enhanced
302 synergism with PU.1 in that the complex induces a faster chromatin opening than the C/EBP α ^{WT}-
303 PU.1 complex, coincident with stronger activation of macrophage markers and induced cell
304 morphology changes.

305 **C/EBP α ^{R35A} hastens the relocation of PU.1 from B cell to macrophage enhancers during** 306 **BMT induction**

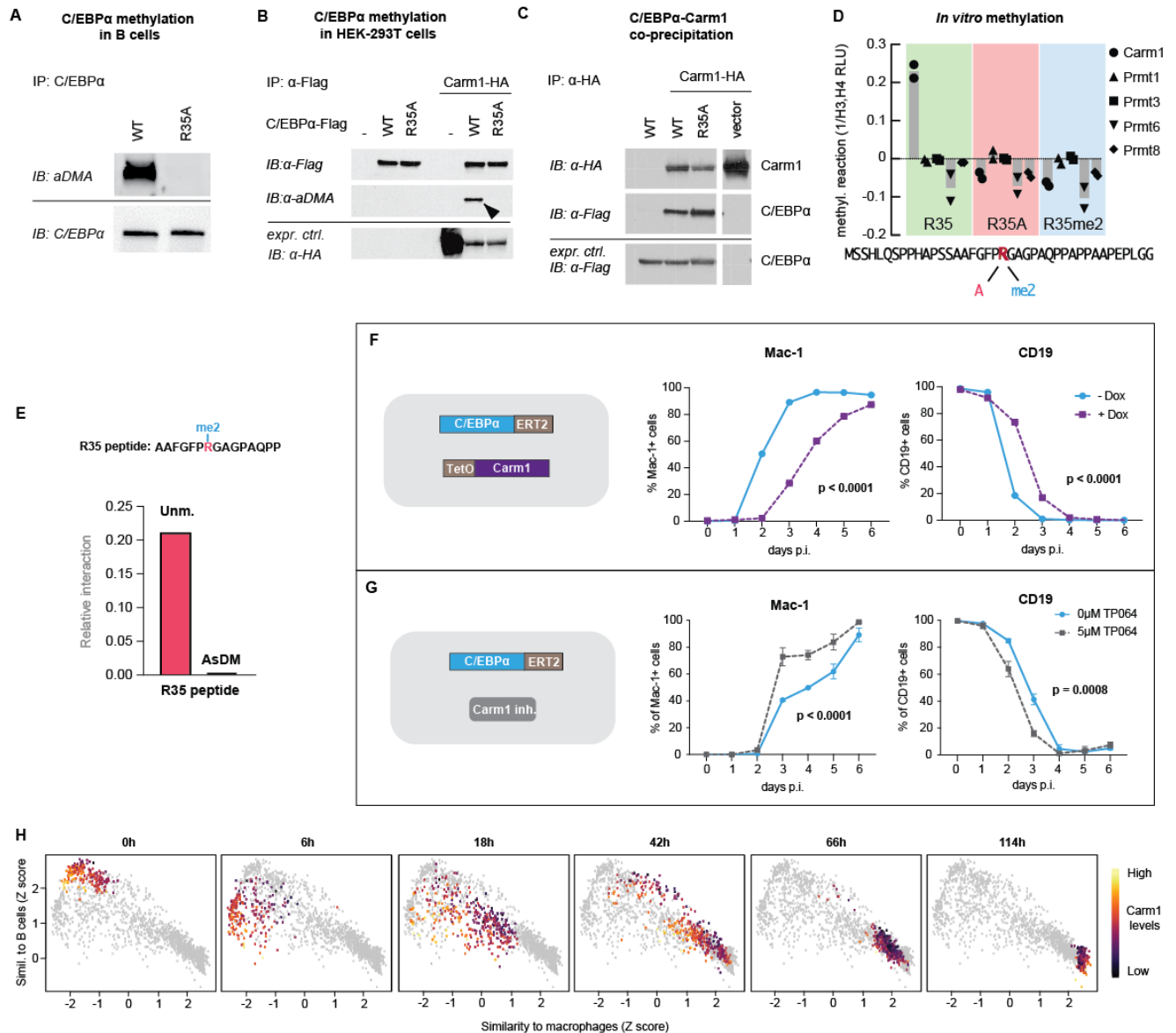
307 The data described raised the possibility that C/EBP α causes a relocation of PU.1 from B cell to
308 macrophage regulatory regions and that the mutant, through its enhanced interaction with PU.1,
309 is more efficient at doing so. This hypothesis predicts that C/EBP α ^{R35A} binding to GREs occupied
310 by PU.1 should induce stronger changes in chromatin accessibility than C/EBP α ^{WT}, while sites
311 devoid of PU.1 should behave more similarly. To test this, we performed a virtual ChIP-seq
312 analysis of C/EBP α and PU.1 during BMT, combining previously generated ChIP-seq data (van
313 Oevelen et al., 2015) with our new ATAC-seq data. We first identified regions stably bound by
314 C/EBP α throughout BMT and then distinguished sites already occupied by PU.1 from PU.1-free
315 sites. This revealed that C/EBP α ^{R35A} induces a significant acceleration of chromatin *opening* at
316 PU.1-bound regions compared to C/EBP α ^{WT}, while regions bound by C/EBP α alone showing

317 much smaller differences (**Figure 4E**). Next, we focused on sites where PU.1 is removed by
318 transiently bound by C/EBP α , distinguishing them from sites where PU.1 is removed yet no
319 C/EBP α binding was detected at any timepoint. This showed that transient binding of C/EBP α ^{R35A}
320 accelerated PU.1 displacement and chromatin closing at PU.1-bound regions. In contrast,
321 although PU.1 was also still removed at sites not targeted by C/EBP α , the effect was much milder
322 (**Figure 4F**).

323 Altogether, our results are consistent with the hypothesis that during BMT, C/EBP α ‘steals’
324 endogenous PU.1 from B cell GREs and relocates it to myeloid GREs. This stealing is
325 exacerbated by C/EBP α ^{R35A}, which is able to more efficiently relocate PU.1 and thus accelerate
326 the conversion of PU.1 from a B cell regulator to a myeloid regulator, in line with the SMT results
327 obtained in fibroblasts.

328 **Carm1 asymmetrically dimethylates arginine 35 of C/EBP α and decreases its affinity for** 329 **PU.1**

330 The finding that a mutation in a specific arginine of C/EBP α is responsible for the observed
331 BMT acceleration raised the possibility that the phenotype is caused by the loss of its potential
332 to be methylated. Since asymmetric dimethylation is one of the most common arginine
333 modifications (Bedford and Clarke, 2009; Bedford and Richard, 2005), we first determined
334 whether R35 is asymmetrically dimethylated. To this end, we generated two cell lines named
335 BLaER2 and BLaER2-A, derived from the B-ALL line RCH-ACV (Jack et al., 1986) expressing
336 the 4-hydroxytamoxifen (4-OHT)- inducible constructs C/EBP α ^{WT}-ERT2 and C/EBP α ^{R35A}-ERT2,
337 respectively. We then induced these cells for 24h with 4-OHT, immunoprecipitated C/EBP α , and
338 ran a Western with an antibody specific for asymmetrically dimethylated arginine (aDMA)-
339 containing proteins. The antibody detected C/EBP α ^{WT} but not C/EBP α ^{R35A}, thus revealing that
340 arginine 35 is asymmetric dimethylated (**Figure 5A**). We next co-transfected HEK293-T cells
341 with either C/EBP α ^{WT} or C/EBP α ^{R35A} and several type I Prmts, namely Prmt1, 3, 4 (Carm1) and
342 6; and assessed the methylation status of C/EBP α . Only Carm1 was able to induce methylation
343 of C/EBP α ^{WT} while C/EBP α ^{R35A} remained unmethylated (**Figures 5B, S5A**).



344

345

346

347

348

349

350

351

352

353

354

355

Figure 5. Carm1 asymmetrically dimethylates arginine 35 and regulates the speed of C/EBPα-induced BMT.

A. Immunoprecipitation (IP) and immunoblotting (IB) of C/EBPα and asymmetrically dimethylated arginine (aDMA) containing proteins. **B.** Immunoprecipitation of C/EBPα from HEK293T cells co-transfected with either C/EBPα^{WT}-Flag or C/EBPα^{R35A}-Flag with or without Carm1-HA, followed by immunoblot with antibodies against aDMA, Flag and HA. **C.** Immunoprecipitation of Carm1 from HEK293T cells co-transfected with either C/EBPα^{WT}-Flag or C/EBPα^{R35A}-Flag and Carm1-HA, followed by immunoblot with antibodies against Flag and HA. **D.** *In vitro* methylation assays with recombinant Carm1, Prmt1, Prmt3, Prmt6 or Prmt8 proteins together with C/EBPα peptides (aa 15-54) that contain either unmethylated arginine 35 (green), with an alanine replacement (A, magenta), or asymmetrically dimethylated (me2, cyan) (mean and individual values are displayed, n=2). **E.** Interaction with PU.1 of a 14-mer peptide (top) containing either an unmethylated (Unm.) or an asymmetrically dimethylated arginine (me, AsDM). The data were extracted from (Ramberger et al., 2021). **F.** Effect of Carm1 overexpression on BMT kinetics

356 of human B cells measured by Mac-1 and CD19 expression (mean \pm s.d., n=3, statistical significance was
357 determined using two-way ANOVA). **G.** Same as F, but effect of Carm1 inhibition by 5 μ M of TP064. **H.** Correlation
358 of Carm1 expression levels in single cell trajectories with B cell and macrophage states. Data extracted from
359 previously published work (Francesconi et al., 2019).

360 To rule out the possibility that the R35 mutation is impaired in its interaction with Carm1 we
361 performed Co-IP experiments in HEK293-T cells co-transfected with Carm1 and either
362 C/EBP α ^{WT} or C/EBP α ^{R35A}, which showed that both proteins are able to interact with the enzyme
363 (**Figure 5C**). To quantitatively assess the interaction of C/EBP α ^{WT} and C/EBP α ^{R35A} with Carm1
364 we performed a PLA assay. For this, NIH3T3 cell lines carrying ER fusions of C/EBP α ^{WT} and
365 C/EBP α ^{R35A} were induced with β -est for 24 hours and subjected to the assay, involving staining
366 with antibodies to C/EBP α and PU.1. We observed nuclear dots in both lines, with slightly higher
367 numbers in C/EBP α ^{R35A} cells, supporting the notion that both forms of C/EBP α can interact with
368 Carm1 (**Figure S5B**).

369 To further assess the enzyme's specificity, we performed an *in vitro* methylation assay using
370 synthetic peptides (10-14-mers), covering all 20 arginine residues of C/EBP α . Only the peptide
371 containing arginine 35 showed a methylation signal (**Figure S5C**). We also performed an *in vitro*
372 methylation assay using a C/EBP α peptide spanning amino acids 15-54 and containing either
373 unmethylated R35, asymmetrically di-methylated R35 or an alanine replacement in the presence
374 of either Carm1, Prmt1, Prmt3, Prmt6 or Prmt8. Only Carm1 was able to methylate the peptide
375 with the original arginine, while no methylation was detected with the other Prmts and with
376 peptides containing methylated R35 or an alanine replacement (**Figure 5D**). Finally, we
377 investigated whether the methylation status of C/EBP α affects its affinity for PU.1, analyzing the
378 interaction data from a peptide motif-based C/EBP α interactome screen (Protein interaction
379 Screen on Peptide Matrix, PRISMA) (Ramberger et al., 2021) comparing an unmethylated
380 peptide with a peptide containing an asymmetrically dimethylated arginine. This showed an
381 impaired interaction of PU.1 with the methylated compared to the unmethylated peptide (**Figure**
382 **5E**).

383 These results indicate that Carm1 selectively targets arginine 35 of C/EBP α and that the
384 Carm1-mediated asymmetric dimethylation of this residue decreases the factor's affinity for
385 PU.1.

386 **Carm1-mediated methylation of arginine 35 modulates C/EBP α -induced BMT**

387 To test the effect of Carm1-mediated methylation of C/EBP α on the factor's ability to induce
388 BMT, we performed Carm1 gain and loss of function experiments. First, we generated a stable
389 derivative of the BLaER2 cell line (named RRC3) that contains the reverse tetracycline
390 transactivator and a doxycycline (Dox)-inducible Carm1 construct. A Western blot confirmed
391 robust Carm1 expression 24 hours after Dox treatment (**Figure S5D**). Assessing the effects of
392 Carm1 overexpression on the kinetics of 4-OHT-induced BMT showed a dramatic delay in both
393 Mac-1 activation and CD19 silencing (**Figure 5F, S6A**). Next, we tested the effect of the Carm1
394 inhibitor TP064 (Nakayama et al., 2018). After verifying that 5 μ M of the drug impairs the
395 asymmetric dimethylation of BAF155 (**Figure S5E**), a known target of Carm1 (Wang et al., 2014)
396 we found that 4-OHT-induced RRC3 cells treated with 5 μ M TP064 resulted in a strongly
397 accelerated BMT (**Figures 5G, S6B**). In contrast, and importantly, C/EBP α ^{R35A}-mediated BMT
398 was not delayed by Carm1 overexpression (**Figures S5F, S6C**) nor did the Carm1 inhibitor cause
399 an acceleration (**Figures S5G, S6D, E**).

400 Our results therefore indicate that high Carm1 expression levels cause a delay in the
401 kinetics of C/EBP α -induced BMT by methylating R35 of the wild type protein, in line with the
402 findings obtained with C/EBP α mutant.

403 **Differences of endogenous Carm1 expression correlate with the speed of BMT induction**

404 To investigate the effect of naturally occurring differences in Carm1 expression on BMT
405 velocity, we used a previously generated single-cell gene expression dataset of cells undergoing
406 BMT (Francesconi et al., 2019). For this, we monitored Carm1 expression during the BMT
407 trajectory of single cells by following their similarity to either B cells or macrophages. This showed
408 that cells with the lowest Carm1 levels were faster in acquiring a macrophage-like identity than
409 cells with higher levels (**Figure 5H**). The differences leveled off between 42 and 66 hpi,
410 suggesting that the largest differences occur in the early stages of BMT, in line with the
411 observation that the kinetics of altered gene expression induced by C/EBP α ^{WT} and C/EBP α ^{R35A}
412 differ mostly at the beginning of the process (**Figure 1F**). These results further support the notion
413 that Carm1-mediated methylation of arginine 35 modulates the velocity of C/EBP α -induced BMT.

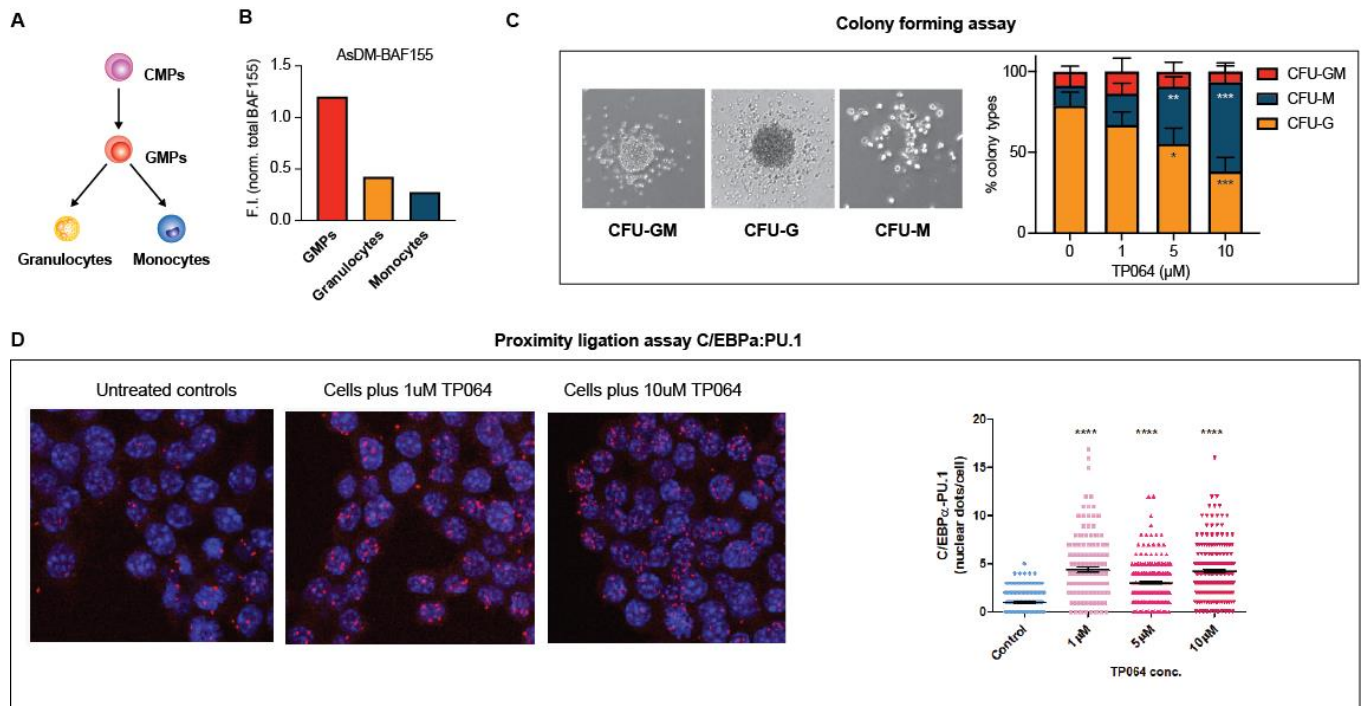
414 **Carm1 inhibition biases GMPs to differentiate towards macrophages**

415 To assess the potential of Carm1 to regulate cell fate decisions during normal myelopoiesis
416 (**Figure 6A**), we investigated Carm1 RNA expression levels in different myeloid precursors as
417 well as granulocytes and macrophages, using a dataset obtained earlier (Choi et al., 2019). This
418 revealed a gradual decrease of Carm1 during the transition from common myeloid progenitors
419 (CMPs) over GMPs to monocytes and granulocytes (**Figure S7A**). Next, we monitored the levels
420 of AsDM-BAF155 as a proxy for Carm1 activity in sorted GMPs, granulocytes and monocytes
421 relative to total BAF155. We observed the highest relative levels of AsDM-BAF155 in GMPs and
422 a 3.5- and 4.5-fold reduction in granulocytes and monocytes, respectively (**Figure 6B, Figure**
423 **S7B**). These results suggest that Carm1 RNA levels and enzymatic activity decrease during
424 myeloid differentiation, reaching their lowest levels at in monocyte/macrophages.

425 To determine whether Carm1 activity affects the decision of GMPs to differentiate into either
426 granulocytes or monocytes, we tested the effect of the Carm1 inhibitor TP064 in a colony assay.
427 For this, we isolated GMPs from mouse bone marrow and seeded them in a semisolid medium
428 containing IL-3 and IL-6 in the presence of 0, 1, 2.5 or 10 μ M TP064. Scoring the number of the
429 different myeloid colony types 12 days later showed a dose-dependent reduction of granulocytic
430 colonies (CFU-G; $p=0.001$) and a concomitant increase of monocytic colonies (CFU-M;
431 $p=0.0003$), with no effect on mixed colonies (CFU-GM; $p=0.506$) (**Figure 6C**). This bias is unlikely

432 due to a granulocyte-selective cytotoxicity of the inhibitor since the total number of colonies
 433 remained essentially constant (**Figure S7C**).

434



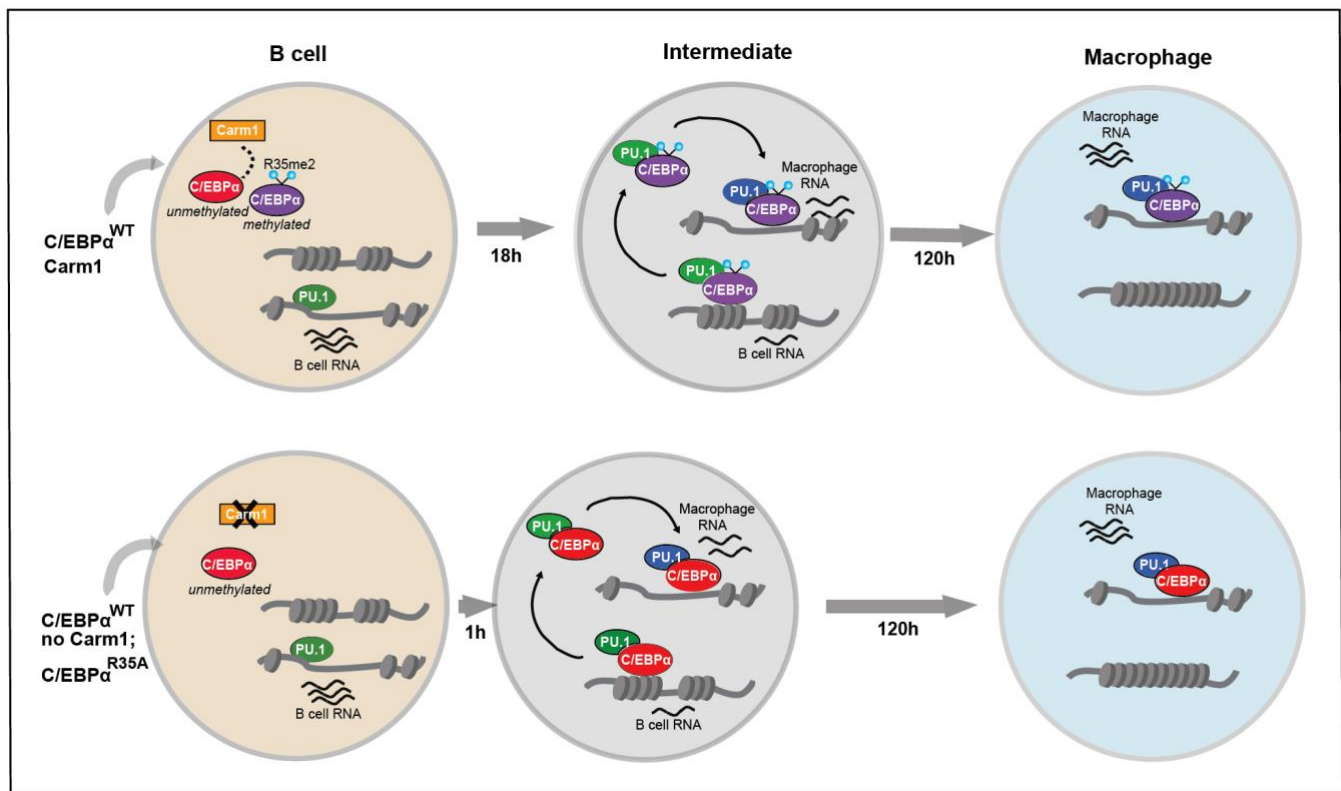
435

436 **Figure 6. Effect of Carm1 activity on myeloid differentiation and C/EBP α -PU.1 interaction.** **A.** Simplified
 437 representation of myeloid differentiation. Common myeloid progenitors (CMPs); granulocyte-macrophage
 438 progenitors (GMPs). **B.** Levels of asymmetrically dimethylated BAF155 (AsDM-BAF155) relative to total BAF155 in
 439 GMPs, granulocytes and monocytes as a proxy for Carm1 activity (see also **Figure S7B**). **C.** On the left,
 440 representative images of colony types obtained from GMPs grown in Methocult. On the right, quantification of colony
 441 numbers obtained in cultures without or with various concentrations of the Carm1 inhibitor TP064 for 14 days,
 442 showing percentage of bipotent (CFU-GM), monocytic (CFU-M) and granulocytic (CFU-G) colonies (mean \pm s.d.,
 443 $n=3-4$, statistical significance was determined using a one-way ANOVA for each cell type) (See also **Figure S7C**).
 444 **D.** Proximity ligation assay of endogenous C/EBP α and PU.1 in the mouse macrophage cell line RAW 264.7 treated
 445 for 24 hours with 1, 5 or 10 μ M TP064 or left untreated. On the left confocal microscopy images. On the right, counts
 446 of nuclear dots per cell (mean \pm s.e., $n=149-190$ cells per condition). Four stars: $P<0.0001$ (statistical significance
 447 determined using an unpaired Student's t-test.).

448 Together, our results suggest that Carm1 modulates the directionality of GMPs, with
 449 unmethylated C/EBP α biasing them to differentiate towards the monocytic lineage and implying
 450 a role of methylated C/EBP α for the granulocytic lineage.

451 **Carm1 inhibition increases interaction between endogenous C/EBP α and PU.1**

452 The experiments described so far, showing an increased affinity between C/EBP α with a
 453 mutated or an unmethylated R35 and PU.1, were performed after C/EBP α overexpression. To
 454 determine whether an increase in affinity can also be observed between endogenous C/EBP α
 455 and PU.1 we tested the effect of Carm1 inhibition on the mouse macrophage line RAW 264.7
 456 (Raschke et al., 1978). For this, the cells were cultured either in the absence or in presence of
 457 1,5 or 10uM of TP064 and subjected to a PLA assay. We observed low numbers of nuclear dots
 458 in the untreated cells and a 4 to 5 fold increase in both cultures treated with the inhibitor (**Figure**
 459 **6D**). This increase was not due to elevated levels of the two proteins in the presence of the
 460 inhibitor, as shown by similar immunofluorescence intensities of C/EBP α and PU.1 (**Figure S7D**).
 461 We conclude that Carm1 inhibition increases the interaction between endogenous C/EBP α and
 462 PU.1, using a macrophage line that expresses similar levels of the two proteins.



463

464 **Figure 7. Proposed mechanism of how Carm1 modulates the velocity of BMT.** The diagram shows the
 465 differences in velocity between a BMT induced by methylated and unmethylated forms of C/EBP α . In condition 1,
 466 cells are induced with C/EBP α ^{WT} in the presence of Carm1 (upper part). In condition 2 (lower part) cells are induced
 467 with either C/EBP α ^{WT} in the absence of Carm1 or with C/EBP α ^{R35A}. Note the more rapid conversion into an
 468 intermediate in the second condition. We hypothesize that C/EBP α induces gene silencing by transiently binding to
 469 gene regulatory elements (GREs) of B cells occupied by PU.1 and other B cell transcription factors. This leads to

470 the release of the C/EBP α :PU.1 complex (and probably the other B cell factors) and chromatin closing. C/EBP α :PU.1
471 complexes then relocate to myeloid GREs, where they induce chromatin opening and activation of macrophage
472 gene expression. Carm1-mediated methylation of arginine 35 delays the BMT by impairing the interaction of C/EBP α
473 with PU.1 and relocation of PU.1 to myeloid GREs. The green symbol for PU.1 implies its role as a B cell regulator,
474 blue as a myeloid regulator.

475 **DISCUSSION**

476 Here we describe a mechanism by which the speed of a hematopoietic cell fate decision is
477 modulated. Using a model system in which C/EBP α induces a B cell to macrophage
478 transdifferentiation (BMT) we found that an arginine 35 mutant dramatically accelerates the
479 process. As summarized in Figure 7, our data, together with that of earlier work (van Oevelen et
480 al., 2015) suggest that C/EBP α initiates B cell gene silencing by binding to specific GREs, a
481 subset of which occupied by PU.1 in addition to B cell restricted regulatory factors. This binding
482 is transient and leads to the rapid release of the complex from chromatin by an unknown
483 mechanism. The free C/EBP α -PU.1 complex in turn translocates to macrophage-specific GREs,
484 inducing chromatin opening and the activation of myeloid genes. During this relocation, PU.1
485 essentially switches from a B cell regulator to a myeloid regulator, now binding to a set of largely
486 myeloid-specific GREs. The speed of this conversion is regulated by the levels of Carm1 in the
487 starting cell, which determines the proportion of methylated or unmethylated arginine C/EBP α at
488 R35. In this stealing model the C/EBP α ^{R35A} mimics the unmethylated form of the factor, showing
489 a stronger affinity for PU.1 than wild type C/EBP α . The model however, does not explain how
490 PU.1 becomes removed from B cell GREs that are not detectably bound by C/EBP α .

491 The observed near symmetrical acceleration of activation and silencing of B cell and
492 myeloid-restricted genes induced by C/EBP α ^{R35A} or by C/EBP α ^{WT} in cells with reduced Carm1
493 activity suggests that PU.1 acts as a cell fate coordinator, preventing the formation of cells with
494 aberrantly regulated lineage programs. Whether during the C/EBP α -induced BMT PU.1 acquires
495 a different conformation when it turns from a B cell to a myeloid regulator will be interesting to
496 determine. A critical parameter for the enhancement of myeloid differentiation during the
497 conversion of a fetal liver T cell precursor into macrophages has been described to be cell cycle
498 length, with cell cycle extension leading to the accumulation of high PU.1 levels (Kueh et al.,
499 2013). Whether under physiological conditions this lengthening is induced by the activation of

500 endogenous C/EBP α , itself known to be a potent inhibitor of the cell cycle (Nerlov, 2007), and
501 whether it is exacerbated by a mutation of R35 remains to be studied.

502 A transcription factor stealing mechanism has also been described for T cell differentiation.
503 Thus, at the DN1 progenitor stage PU.1 forms a complex with Satb1 and Runx1 at GREs of
504 PU.1-dependent genes. Once PU.1 becomes downregulated at the DN3 stage, the associated
505 factors are released and relocate to T cell GREs where they upregulate T cell genes (Hosokawa
506 et al., 2018). However, in contrast to the mechanism described here, where C/EBP α acts as the
507 ‘thief’ and PU.1 as the ‘victim’, PU.1 is the ‘thief’. In another relevant example T-bet relocates
508 Gata3 from T_H2 to T_H1 genes during TH1 specification (Hertweck et al., 2022). These studies
509 support the notion that transcription factor ‘stealing’ could be a more general mechanism by
510 which cells coordinate silencing of the old and activation of the new differentiation program.

511 Remarkably, C/EBP α ^{R35A} expression in B cells generates a myeloid cell-like state already
512 within 1 hpi, only seen with the wild type after 18 hpi. Whether the observed catching up in gene
513 expression after 120 h in C/EBP α ^{WT}- induced cells occurs gradually or in a more narrowly defined
514 time window remains to be determined. Reflecting these observations, the capacity of C/EBP α
515 to induce a transition of closed to open chromatin in fibroblasts is remarkably fast compared to
516 other pioneer transcription factors (Lerner et al., 2020). That co-expression of PU.1 further
517 accelerates chromatin opening in fibroblasts while activating the myeloid program suggests a
518 powerful synergism between the two pioneer factors, regulated by methylation of arginine 35.
519 BMT completion requires 3 to 5 days for mouse cells while human cells require 5 to 7 days
520 (Rapino et al., 2013; Xie et al., 2004), raising the possibility that species-specific differences in
521 Carm1 activity play a role. However, the observation that inhibition of Carm1 accelerates BMT
522 not only in human but also in mouse cells makes this unlikely. It will be interesting to determine
523 whether the observed species differences of BMT length reflects a higher protein stability in the
524 human cells, as reported for neuronal specification (Rayon et al., 2020), although other
525 mechanisms have also been described (Ebisuya and Briscoe, 2018).

526 In line with the results described here that Carm1 inhibition biases GMPs to differentiate into
527 macrophage colonies, HSCs lacking Carm1 have been shown to be biased towards monocyte
528 formation (Greenblatt et al., 2018). These observations suggest that methylated C/EBP α is
529 required for the decision of GMPs to become granulocytes, and that this form of the factor is not

530 simply inactivated during macrophage specification. A role of transcription factor methylation by
531 Carm1 has also been described for muscle differentiation. Here, asymmetric dimethylation of
532 four arginines in Pax7 enables recruitment of the MLL complex. As a consequence, Myf5
533 becomes transcriptionally activated, resulting in muscle cell specification (Chang et al., 2018;
534 Kawabe et al., 2012). Carm1 has also been implicated in early embryo development and several
535 targets have been described, including histones and chromatin modifying factors (Suresh et al.,
536 2021; M.-E. Torres-Padilla et al., 2007), but whether this also involves the methylation of a key
537 transcription factor is unknown.

538 Our observations challenge the notion that binary cell fate decisions simply result from the
539 relative expression of antagonistic transcription factors (Graf and Enver, 2009; Moris et al., 2016).
540 Rather, post-translational modifications, such as described here, may act as an additional
541 regulatory layer (Torcal Garcia and Graf, 2021). Thus, the proportions of a modified versus
542 unmodified transcription factor within a precursor population could be subject to external
543 signaling that activates Carm1 or another enzyme that induces posttranslational modifications.
544 Such a mechanism could operate regardless of whether binary cell fate decisions occur gradually
545 as reported for hematopoiesis (Velten et al., 2017) or abruptly as during a neuronal differentiation
546 cascade (Konstantinides et al., 2022). How the timing of alternative cell fate decisions is
547 regulated is relevant not only for a better understanding of cell differentiation but also for
548 aberrations in developmental diseases such as certain types of cancer.

549

550 **ACKNOWLEDGEMENTS**

551 We thank the T.G. laboratory members for critical discussions, the Flow Cytometry and
552 Microscopy units of UPF-CRG for technical assistance, the CRG Genomics core facility for
553 sequencing and Lars Velten for feedback on the manuscript. Work in the laboratory of T. G. was
554 supported by the Spanish Ministry of Economy, Industry and Competitiveness, (Plan Estatal
555 PID2019-109354GB-100), the CRG, AGAUR (SGR 726) and a European Research Council
556 Synergy grant (4D-Genome). Work in the laboratory of K.S.Z. was supported by NIH
557 (R01GM36477).

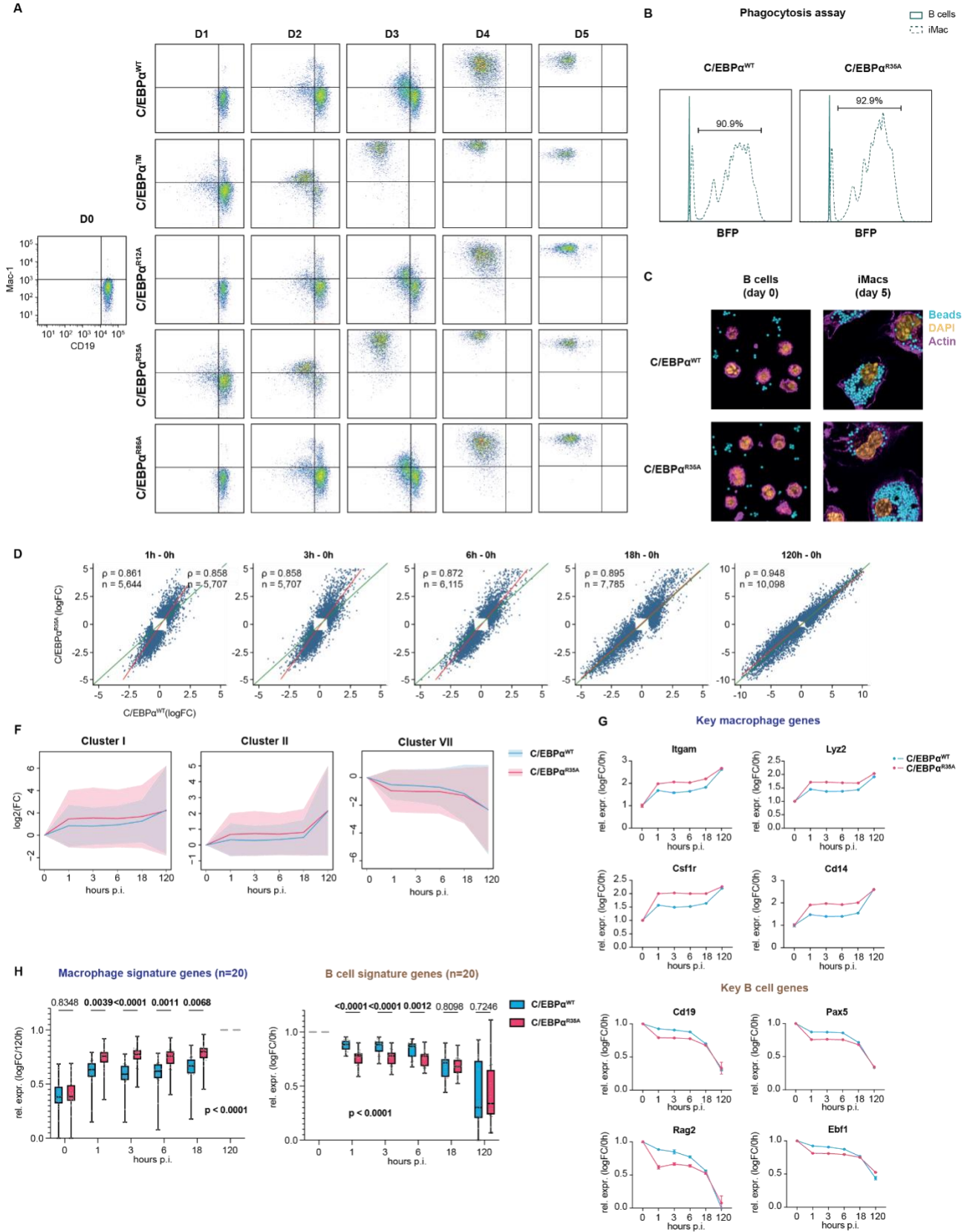
558 **AUTHOR CONTRIBUTIONS**

559 G.T.G and T.G. conceived the study and wrote the manuscript. G.T.G. performed
560 transdifferentiation experiments (BMT and fibroblasts), cell line generation, RNA- and ATAC-seq,
561 plasmid construction, immunofluorescence, and data analyses. E.K-L performed co-
562 immunoprecipitation, EMSA and *in vitro* methylation assays. T.V.T. performed BMT, RNA- and
563 ATAC-seq. A.K. and M.V-C. processed RNA-, ATAC- and CHIP-seq data. J.L. performed SMT
564 experiments. L.A-A. performed co-immunoprecipitation, FACS, PLA and colony assays. C.B-B.
565 performed BMT. M.P-C. confocal microscopy. R.B. and M.F. analyzed single cell expression
566 data. S.P., K.Z., A.L. contributed ideas and discussions.

567

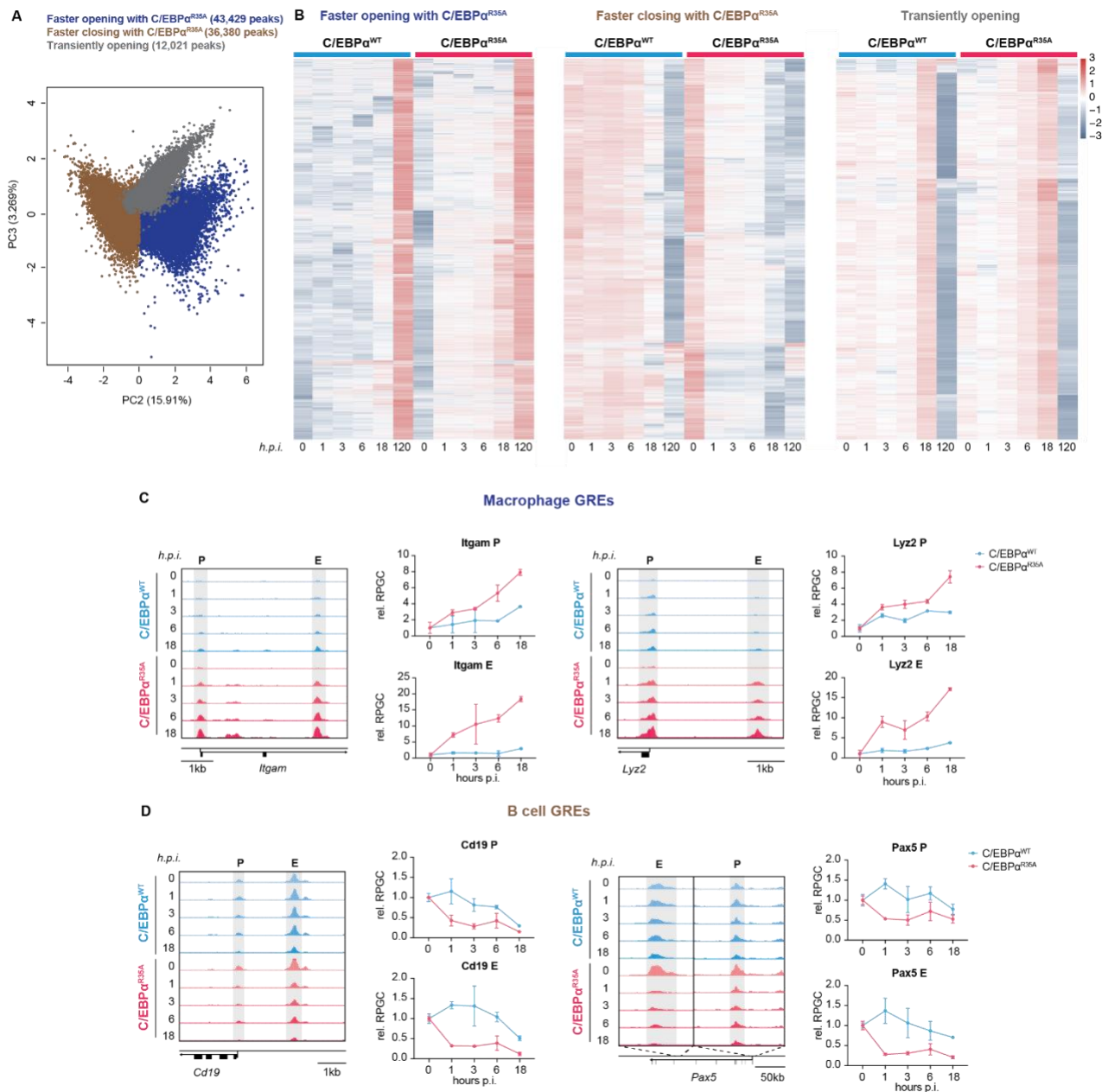
568

569 **SUPPLEMENTAL INFORMATION**



571 **Figure S1. Mutation of arginine 35 in C/EBP α accelerates B cell gene silencing and macrophage gene**
572 **activation. Related to Figure 1. A.** FACS plots of Mac-1 (CD11b) and CD19 expression in B cells induced with
573 C/EBP α^{WT} , C/EBP α^{TM} , C/EBP α^{R12A} , C/EBP α^{R35A} or C/EBP α^{R86A} at different days p.i. **B.** Histograms showing
574 fluorescence intensity of internalized BFP carboxylated beads in C/EBP α^{WT} and C/EBP α^{R35A} -induced cells (dashed
575 line) incubated overnight by flow cytometry. Data for uninduced control B cells are represented by a continuous line.
576 Percentage of phagocytic cells is indicated. **C.** Immunofluorescent images of uninduced (day 0) and 5 days-induced
577 pre B cells incubated overnight with BFP carboxylated beads. DNA was stained with picogreen (P7589) and F-actin
578 with phalloidin Alexa Fluor 568. **D.** Scatter plots showing gene expression changes at 1, 3, 6, 18 and 120 hpi relative
579 to 0h for B cells induced with either C/EBP α^{WT} or C/EBP α^{R35A} . Red line = regression line fitted to each scatter plot;
580 green line = identity line ($x=y$); ρ = Spearman correlation coefficient; n = number of differentially expressed genes.
581 **E.** Kinetics of gene expression of clusters I, II and VII of B cells induced with either C/EBP α^{WT} (cyan) or C/EBP α^{R35A}
582 (magenta) at different times p.i. The Y axis shows log₂ fold-changes relative to uninduced cells. The lines and the
583 shaded backgrounds correspond to the mean \pm 1.64 s.d., $n=1103-1868$. **F.** RNA expression levels of key
584 macrophage or B cell genes in B cells induced by either C/EBP α^{WT} (cyan) or C/EBP α^{R35A} (magenta) relative to 0h
585 (mean \pm s.d., $n=2$). **G.** RNA expression levels of selected macrophage and B cell signature genes in B cells induced
586 by either C/EBP α^{WT} (cyan) or C/EBP α^{R35A} (magenta) relative to 120h and 0h, respectively (median and quartiles are
587 represented, $n=20$, statistical significance was determined using multiple paired Student's t-test for individual
588 timepoint comparisons as well as Two-way ANOVA for overall statistical significance).

589



590

591

Figure S2. C/EBP α^{R35A} accelerates chromatin remodeling at regulatory elements of lineage-restricted genes.

592

Related to Figure 2. A. PCA analysis of individual peaks showing PC2 and PC3 and the three clusters that were

593

generated ($n = 91,830$ peaks). **B** Three clusters were generated from a PCA analysis shown in A. The clusters show

594

three main trends: regions that are opened throughout BMT, more rapidly so with C/EBP α^{R35A} (blue); regions that

595

are closed throughout BMT, also more rapidly so with C/EBP α^{R35A} (brown); and regions that peak at 18h and are

596

closed at 120h (grey). **C.** Gene ontology (GO) enrichment of macrophage-myeloid and B cell terms of each cluster

597

from Figure 2C. Diameter of circles is proportional to the p-value. Colored circles indicate significant enrichment.

598

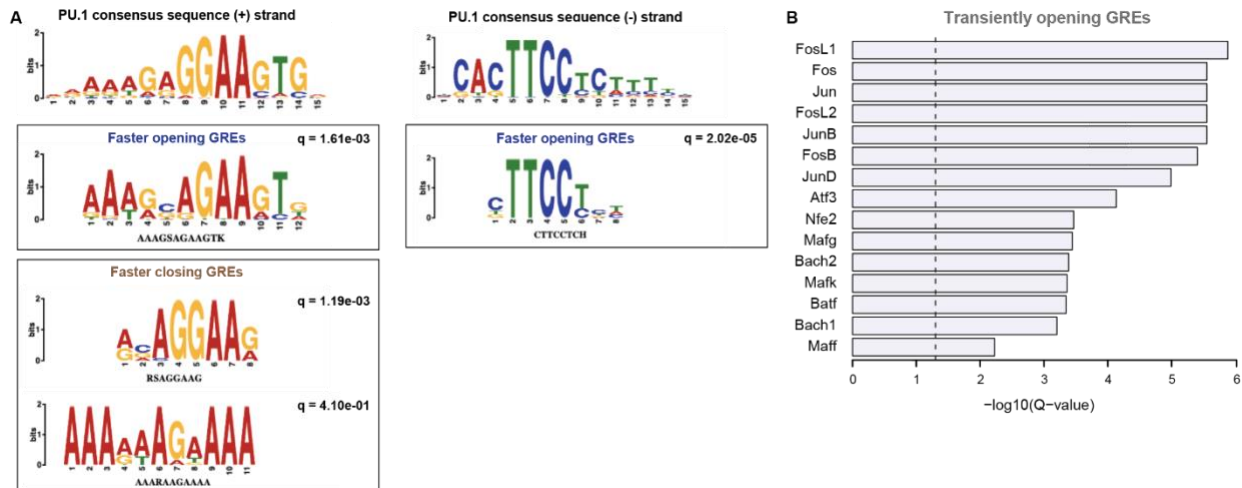
Chromatin accessibility kinetics of key macrophage (**D**) and B cell (**E**) gene regulatory elements (GREs). Genome

599

browser views of ATAC peaks (gray highlight; P=promoter, E=enhancer) corresponding to known or putative GREs

600 of macrophage (*Itgam* and *Lyz2*) and B cell genes (*Cd19* and *Pax5*). Genes, direction of transcription and scale are
601 indicated in each panel. Kinetics of chromatin accessibility at different timepoints are displayed for C/EBP α ^{WT} (cyan)
602 and C/EBP α ^{R35A} (magenta) as reads per genomic content relative to 0h (RPGC).

603

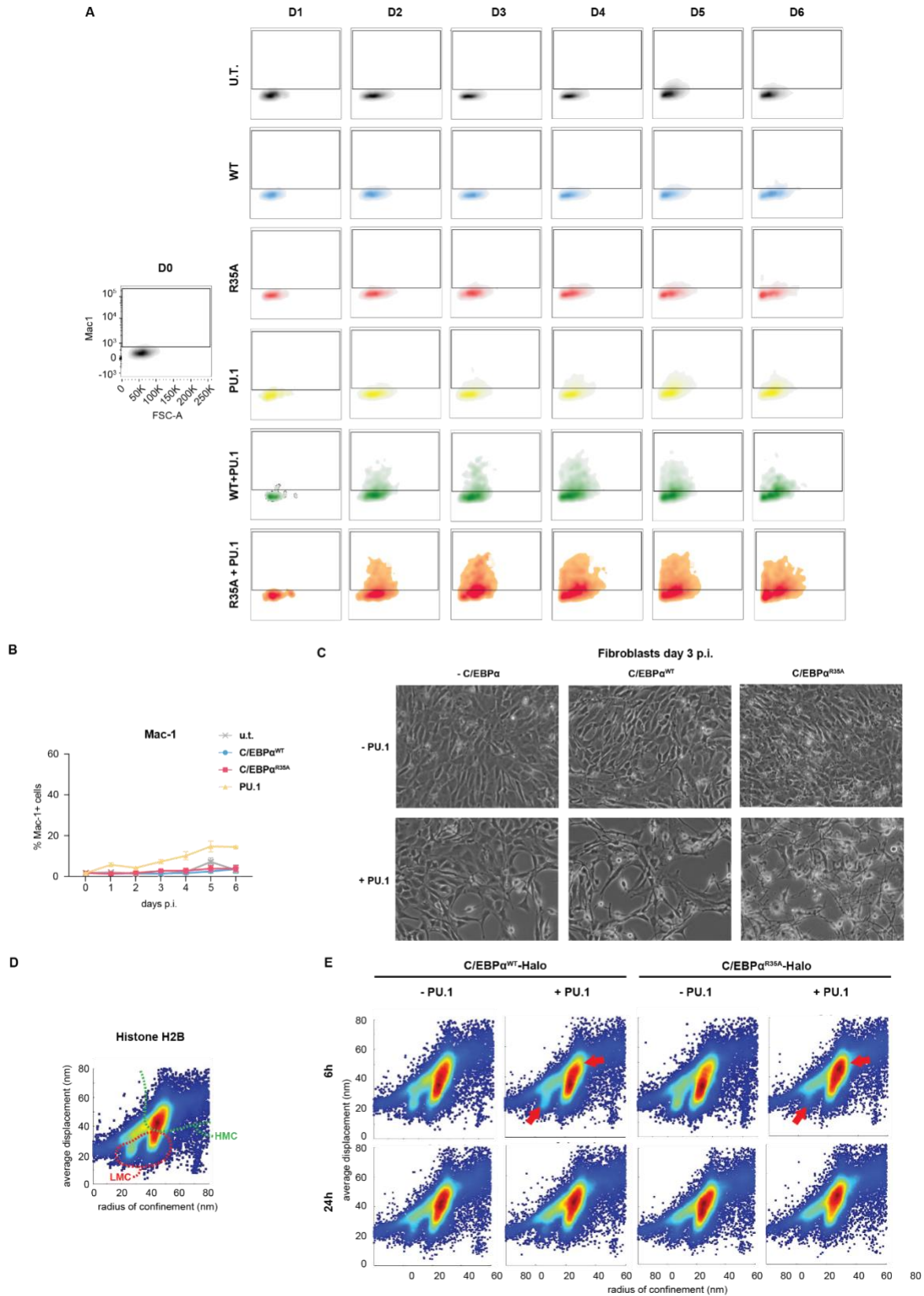


604

605

Figure S3. C/EBP α ^{R35A} selectively interacts with PU.1. Related to Figure 3. A. PU.1 enriched motifs related to Figure 3D. PU.1 consensus sequence in the + and – strand is displayed (top), as well as matched enriched de novo motifs. **B.** De novo motifs matched to known TF motifs in putative in GREs that are transiently opened (grey) obtained in Figure S2A and B. Top 20 motifs are ordered by significance.

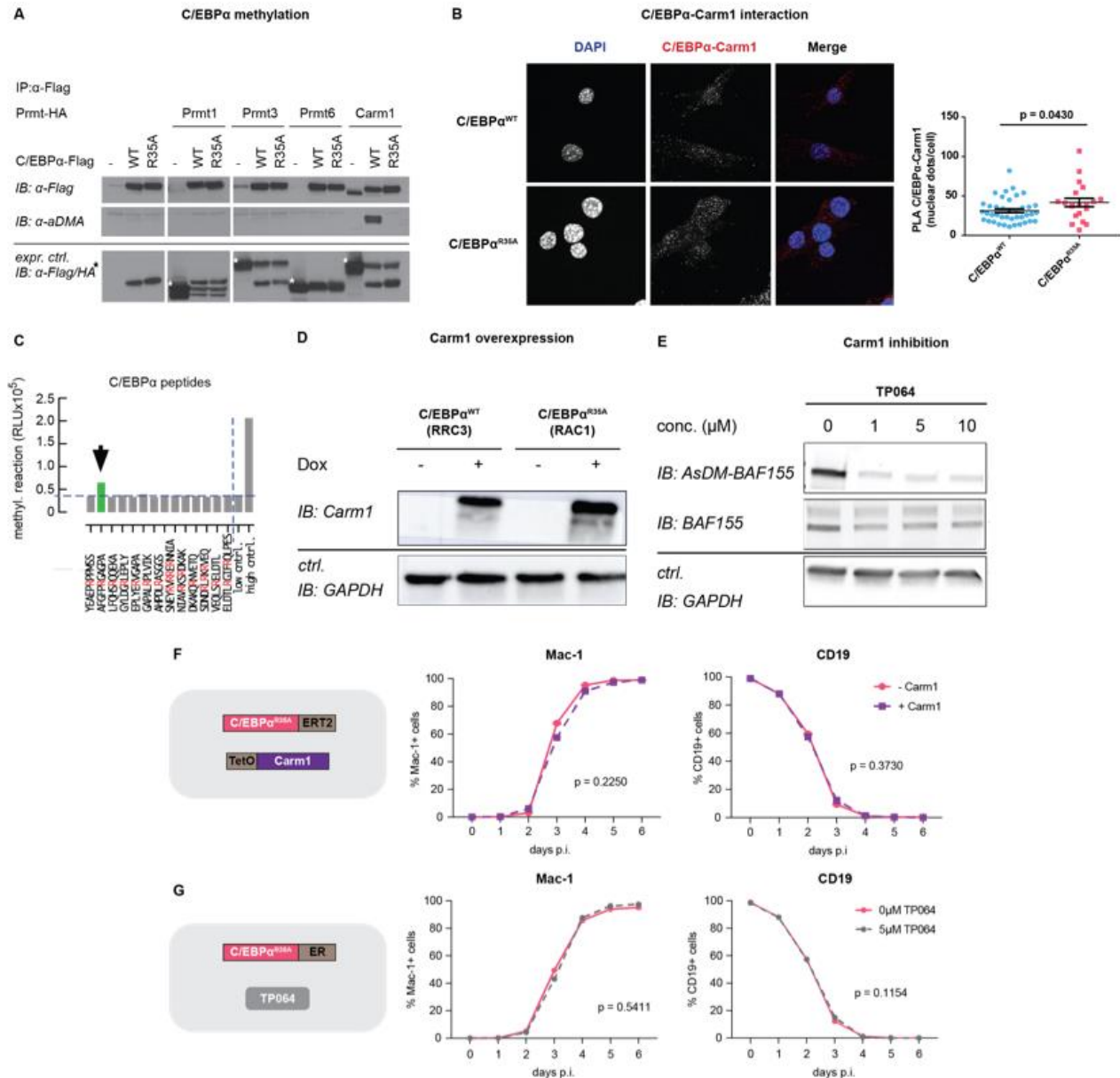
609



610

611 **Figure S4. C/EBP α^{R35A} hastens the relocation of PU.1 from B cell to myeloid GREs. Related to Figure 4. A.**

612 FACS plots of the fibroblast to macrophage transdifferentiation by co-expression of either C/EBP α ^{WT} or C/EBP α ^{R35A}
613 and PU.1 measured by Mac-1 expression by flow cytometry. **B.** Kinetics of macrophage transdifferentiation induced
614 by C/EBP α ^{WT}, C/EBP α ^{R35A} or PU.1 and untransduced cells (u.t.) measured by Mac-1 expression by FACS (mean \pm
615 s.d., n=3, statistical significance was determined using two-way ANOVA). **C.** Phase contrast images of NIH3T3 cells
616 induced with either C/EBP α ^{WT} or C/EBP α ^{R35A} and PU.1 in different combinations for 3 days. **D.** Single molecule-
617 tracking (SMT) of histone H2B in 3T3 cells transfected with an H2B-Halo tag construct for 24h (n = 20,000). Average
618 displacement and radius of confinement are displayed, and chromatin mobility groups were identified (vL = very low;
619 L = low; I = intermediate; H = high). **E.** Single molecule-tracking (SMT) of either C/EBP α ^{WT} or C/EBP α ^{R35A} in 3T3
620 cells infected with a Dox-inducible C/EBP α -Halo constructs for either 6 or 24h with or without PU.1 co-expression
621 (n = 20,000).

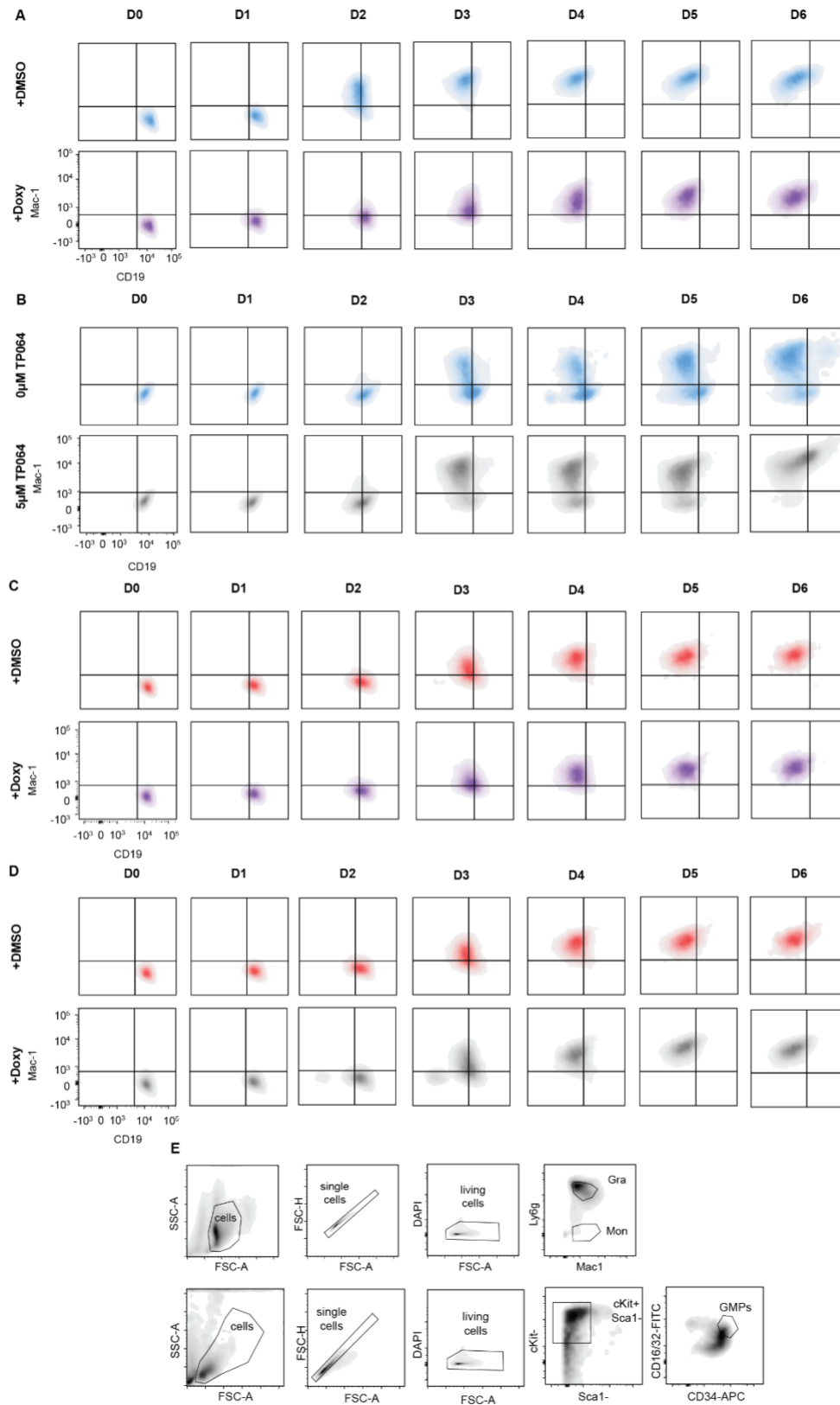


622

623 **Figure S5. Carm1-mediated methylation of arginine 35 regulates interaction between the two proteins and**
 624 **the speed of C/EBP α -induced BMT. Related to Figure 5. A.** Immunoprecipitation of C/EBP α ^{WT} or C/EBP α ^{R35A}
 625 (Flag) from HEK293-T cells co-transfected with either C/EBP α ^{WT}- or C/EBP α ^{R35A}-Flag and different type I Prmt
 626 enzymes (Prmt1, Prmt3, Prmt6 and Carm1), followed by immunoblot with antibodies against asymmetrically
 627 dimethylated arginine (aDMA), Flag or HA. **B.** Proximity ligation assay of Carm1 and C/EBP α ^{WT} or C/EBP α ^{R35A} in
 628 fibroblast lines 3T3aER-R and 3T3aER-A, respectively, induced with β -estradiol for 24 hours. On the left, images of
 629 the cells showing DNA stained with DAPI and interaction between C/EBP α and Carm1. On the right, quantification
 630 of interaction by nuclear dots per cell (mean \pm s.e.; n=20-40, statistical significance was determined using an
 631 unpaired Student's t-test). **C.** In vitro methylation assay using Carm1 and 13 arginine-containing peptides spanning
 632 the entire C/EBP α protein (15 peptides, 20 R-residues highlighted in red). Peptide containing R35 bar indicated in

633 green. Low control: no enzyme; high control: optimized R-methylation peptide, provided by BPS Bioscience) **D.**
634 Western blot of Carm1 in B cell lines RRC3 and RAC1 with or without addition of Dox. **E.** Western blot of
635 asymmetrically dimethylated BAF155 (AsDM-BAF155) and total BAF155 (BAF155) in B cells treated with different
636 concentrations of TP064 (1-10 μ M). **F.** Kinetics of C/EBP α ^{R35A}-mediated BMT upon Carm1 overexpression by pre-
637 treatment with Dox for 24h measured by Mac-1 and CD19 expression by flow cytometry (mean \pm s.d.; n=3, statistical
638 significance was determined using two-way ANOVA). **G.** Kinetics of C/EBP α ^{R35A}-mediated BMT upon Carm1
639 inhibition by pre-treatment with TP064 for 24h measured by Mac-1 and CD19 expression by flow cytometry (mean
640 \pm s.d.; n=3, statistical significance was determined using two-way ANOVA).

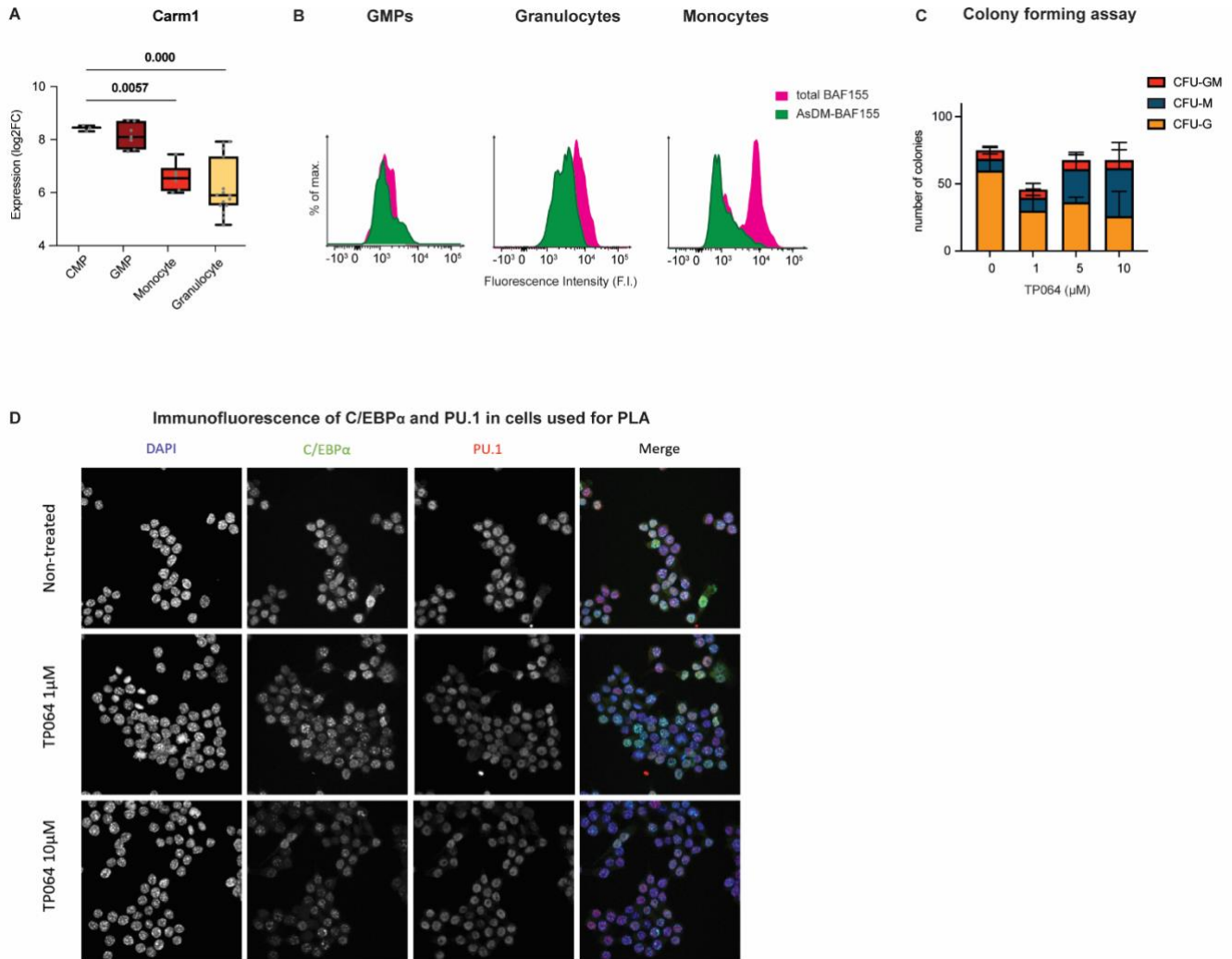
641



642

643 **Figure S6. Carm1-mediated methylation of arginine 35 regulates the speed of C/EBP α -induced BMT. Related**

644 **to Figure 5. A.** FACS plots showing BMT of cells induced with C/EBP α ^{WT} and exposed to Carm1 overexpression
 645 after staining for the lineage markers Mac-1 and CD19. **B.** FACS plots showing BMT of cells induced with C/EBP α ^{WT}
 646 and exposed to 5 μ M TP064 after staining for the lineage markers Mac-1 and CD19. **C.** FACS plots showing BMT of
 647 cells induced with C/EBP α ^{R35A} and exposed to Carm1 overexpression after staining for the lineage markers Mac-1
 648 and CD19. **D** FACS plots showing BMT of induced with C/EBP α ^{R35A} and exposed to 5 μ M TP064 after staining for
 649 the lineage markers Mac-1 and CD19. **E.** Gating strategy for sorting of bone marrow-derived granulocytes,
 650 monocytes (upper panels) and GMPs (lower panels).



651

652 **Figure S7. Dimethylation of C/EBP α by Carm1 is involved in the lineage choice of hematopoietic cells and**
 653 **C/EBP α :PU.1 interaction. Related to Figure 6 A.** Expression of Carm1 during myeloid differentiation obtained
 654 from RNA-seq published data (Choi et al., 2019) (quartiles are represented, n=3-7, statistical significance was
 655 determined using multiple unpaired Student's t-tests). **B.** FACS plots showing levels asymmetrically dimethylated
 656 (AsDM)-BAF155 and total BAF155 in GMPs, granulocytes and monocytes. The histograms represent fluorescence
 657 of each fraction of the protein. **C.** Colony forming unit (CFU) assay of GMPs in various concentrations of the Carm1
 658 inhibitor TP064 after 14 days in Methocult. Total number of bipotent (CFU-GM), monocytic (CFU-M) and granulocytic

659 (CFU-G) colonies are shown (mean \pm s.d., n=3-4, statistical significance was determined using a one-way ANOVA).
660 **D.** C/EBP α and PU.1 fluorescence in RAW cells used for PLA in Figure 6. DNA was stained with DAPI, C/EBP α
661 with AF488 and PU.1 with AF546.

662

663

664 **MATERIALS AND METHODS**

665 **Mice**

666 As a source for the B cells used in our experiments, we used C57BL/6J mice. During experiments
667 the number of female and male mice was balanced. Mice were housed in standard cages under
668 12h light-dark cycles and fed *ad libitum* with a standard chow diet. All experiments were approved
669 by the Ethics Committee of the Barcelona Biomedical Research Park (PRBB) and performed
670 according to Spanish and European legislation.

671 **Cells and cell cultures**

672 CD19+ B cells were isolated from the bone marrow with a monoclonal antibody to CD19 (BD
673 Biosciences, Cat#553784) using MACS sorting technology (Miltenyi Biotech) as previously
674 described (Di Stefano, 2016). Bone marrow-derived B cells were cultured on gelatinized plates
675 containing S17 feeder cells in RPMI culture medium (GIBCO, Cat#12633012) containing 20%-
676 FBS (GIBCO, Cat#10270-106), 100 U/mL Penicillin- 100 ng/mL Streptomycin (GIBCO,
677 Cat#15140122), 2mM L-Glutamine (GIBCO, Cat#25030081) and 0.1mM 2-Mercaptoethanol
678 (Invitrogen, Cat#31350010)(further addressed as **mouse B cell medium**), which was further
679 supplemented with 10 ng/mL of IL-7 (Peprotech, Cat#217-17). HEK293-T, NIH3T3 cells (and
680 derived) and MEFs were cultured in 10% FBS (GIBCO, Cat#10270-106) DMEM (GIBCO,
681 Cat#12491015) medium. The final culture medium also contained 100U/mL Penicillin and
682 100ng/mL Streptomycin (GIBCO, Cat#15140122), 2mM L-Glutamine (GIBCO, Cat#25030081)
683 and 0.1mM 2-Mercaptoethanol (Invitrogen, Cat#31350010) (further addressed as DMEM
684 complete medium). RCH-ACV (and derived) human B cells were grown in RPMI culture medium
685 (GIBCO, Cat#22400089) containing 20%-FBS (10270-106, GIBCO) (further addressed as
686 human B cell medium).

687 **Induction of mouse B cell to macrophage transdifferentiation**

688 Induction of transdifferentiation of primary pre/pro B cells (heretofore referred as B cells) isolated
689 from the bone marrow of C57BL/6J mice was performed as previously described(Xie et al.,
690 2004a). Briefly, B cells isolated from 8-16 weeks C57BL/6J mice were infected with C/EBP α -ER-
691 hCD4 retrovirus, plated at 500 cells/cm² in gelatinized plates (12 wells) onto mitomycin-C (Sigma,
692 Cat#M0503)-treated MEFs (10 μ g/mL mitomycin-C for 3 hours to inactivate MEFs). Cells were
693 transdifferentiated in mouse B cell medium, which was further supplemented with 10 ng/mL each

694 of IL-7 (Peprotech, Cat#217-17), IL-3 (Peprotech, Cat#213-13), FLT-3 (Peprotech, Cat#250-31),
695 mCSF-1 (Peprotech, Cat#315-03B), mSCF (Peprotech, Cat#250-03) and 100 nM β - estradiol
696 (Merck Millipore, Cat#3301) to shuttle C/EBP α into the cell nucleus. Culture medium was
697 renewed every 2 days with the same composition but without IL-7.

698 **Induction of fibroblast to macrophage transdifferentiation**

699 Fibroblast transdifferentiation into macrophage experiments were performed as previously
700 described (Feng et al., 2008b). Briefly, NIH 3T3 fibroblasts were infected with C/EBP α -ER-IRES-
701 hCD4 retrovirus and hCD4 positive cells were sorted and a cell line was established. Cells were
702 plated at 200,000 cells/ml in gelatinized 6-well plates and infected with PU.1 Δ PEST-IRES-GFP
703 retrovirus. After 24 hours cells were re-plated at 30,000 cells/ml in gelatinized 24-well plates in
704 DMEM complete medium supplemented with IL-3 (Peprotech, Cat#213-13) mCSF-1 (Peprotech,
705 Cat#315-03B) and 100 nM β -estradiol (Merck Millipore, Cat#3301) to shuttle C/EBP α into the
706 nucleus.

707 **Induction of human B cell to macrophage transdifferentiation**

708 Transdifferentiation of human B cells from the B lymphoblastic leukemia cell line RCH-ACV was
709 performed as previously described (Rapino et al., 2013b). Briefly, RCH-ACV cells were infected
710 with C/EBP α -ER-IRES-GFP retroviruses and GFP-positive cells were sorted, and clonal lines
711 (BLaER2 and BLaER2-A) were generated. These lines were then infected with rtTA-Puromycin
712 retroviruses and selected with 1 μ g/mL of Puromycin for 1 week. Selected cells were further
713 infected with pHAGE-TetO-Carm1-IRES-dTomato lentiviruses. Cells were grown in human B cell
714 medium, supplemented with 2 μ g/mL of doxycycline (Sigma, Cat#D9891). Tomato-positive cells
715 were sorted, and clonal cell lines were established (RRC3 and RAC1). For transdifferentiation
716 cells were grown in human B cell medium, which was further supplemented with 10 ng/mL each
717 of IL-3 (Peprotech, Cat#200-03), CSF-1 (Peprotech, Cat#315-03B) and 2.5 μ M 4-
718 hydroxytamoxifen (4-OHT) (Sigma, Cat#H7904) to shuttle C/EBP α into the cell nucleus.

719 **Hematopoietic colony forming assay**

720 Bone marrow-derived GMPs from C57BL/6J mice were isolated by FACS sorting and cultured in
721 Methocult GF M3434 (03434, Stem Cell Technologies) for 14 days. Cells were harvested from
722 the Methocult cultures, and colonies were investigated by microscopy.

723 **Cell transfection**

724 HEKT-293T cells were transfected with C/EBP α WT or mutant expression vectors in the absence or
725 presence of PRMT1-HA, PRMR3-HA, CARM1-HA, PRMT6-HA or Pu.1 as indicated using
726 Polyethylenimine according to the manufacturer's protocol (PEI, Polysciences, Cat#24765-2)

727 **Lentivirus production and infection**

728 Lentiviruses were produced by transfecting HEK-293T cells with 6 μ g of pCMV-VSV-G, 15 μ g of
729 pCMVDR-8.91, and 20 μ g of the lentiviral vector using the calcium phosphate transfection
730 method. Briefly, calcium phosphate-DNA precipitates were prepared by pooling the upper
731 amounts of the three plasmids in a 2.5M CaCl₂ aqueous solution. While vortexing, one volume
732 of HBS 2X (HEPES-buffered saline solution pH=7.05, 280mM NaCl, 0.05M HEPES and 1.5mM
733 Na₂HPO₄) was added dropwise to an equal volume of the calcium phosphate-DNA solution.

734 The mixture was incubated for 15 minutes at room temperature and added dropwise to HEK-
735 293T cells grown in DMEM complete medium onto gelatin-coated 100mm dishes. After 8 hours
736 of incubation at 37°C, the transfection medium was replaced with fresh medium and the
737 supernatant collected after 24 hours. The medium was replaced again, and a second round of
738 supernatant was collected after another 24 hours and mixed with the previous batch. The
739 combined supernatants were centrifuged for 5 min at 300 rcf and filtered through 0.45 μ m
740 strainers to remove cell debris. Lentiviral particles were then concentrated by centrifugation for
741 2 hours at 20,000 rcf (Beckman Coulter, Optima L-100K) in round bottom polypropylene tubes
742 (Beckman Coulter, Cat#326823). After discarding the supernatants, the lentiviral pellets obtained
743 from one 150mm dish were thoroughly re-suspended in 80 μ L of PBS. 10⁶ fresh cells were then
744 collected in 900 μ L of the respective culture medium and 10 μ L of lentiviral suspension were
745 added. Subsequently, the virus-cell mixture was centrifuged at 1,000 rcf for 2 hours at 32°C
746 (Beckman Coulter, Allegra X- 30R). Infected cells were then cultured as described above and
747 subsequently FACS-sorted for the establishment of clonal cell lines.

748 **Retrovirus production and infection**

749 Retrovirus constructs were generated as described before (Bussmann et al., 2009). For
750 production of virus for mouse cells platinum E cells (Cell Biolabs, Cat#RV-101) were transfected.
751 Platinum A cells (Cell Biolabs, Cat#RV-102) were transfected for human cells. Infection of cells
752 was performed as previously described (Di Stefano et al., 2014).

753 **Carm1 inhibition experiments with TP064**

754 TP064 (Bio-Techne RD Systems, Bristol, UK) was used to inhibit Carm1 activity as previously
755 described (Nakayama et al., 2018). For experiments with B cells, these were pre-incubated with
756 5 μ M of TP046 24 hours prior to induction with β -est, and treatment with the inhibitor continued
757 during the time of induction. For the colony forming assay with GMPs, 1-10 μ M of TP064 was
758 added to the medium at the time of plating.

759 **Cell purification**

760 Mouse bone marrow cell extraction was performed as previously described (Di Stefano et al.,
761 2014). Briefly, femurs and tibias of C57BL/6J mice were extracted and crushed on a mortar in
762 PBS supplemented with 4%FBS and 2 mM EDTA and filtered through 0.45 μ m strainers (Merck
763 Millipore, Cat#SLHV033RB). For B cells, bone marrow-derived cells were incubated with
764 sequentially 0.1 μ g per 1 million cells of both Fc block and Cd19-Biotin antibody for 10 and 20
765 minutes respectively, followed by 10 μ L of magnetic streptavidin microbeads (Miltenyi, Cat#130-
766 048-101) for an additional 20 minutes. Cd19+ cells were sorted using LS columns (Miltenyi,
767 Cat#130-042-401). For B cell to macrophage transdifferentiation Cd19+ B cells were infected
768 with C/EBP α -ER-IRES-hCD4 (WT and mutants) and cultured over MEF feeder cells for 4 days.
769 Cultured B cells were incubated sequentially with 0.1 μ g per 1 million cells of both Fc block and
770 hCD4-Biotin antibody for 10 and 20 minutes respectively, followed by 10 μ L of magnetic
771 streptavidin microbeads (Miltenyi, Cat#130-048-101) for an additional 20 minutes. hCD4+ cells
772 were enriched with LS columns (Miltenyi, Cat#130-042-401).

773 For granulocytes and monocytes, bone marrow-derived cells were incubated sequentially
774 with 0.1 μ g per 1 million cells of both Fc block and Mac1-Biotin antibody for 10 and 20 minutes
775 respectively, followed by 10 μ L of magnetic streptavidin beads (Miltenyi, Cat#130-048-101) for
776 an additional 20 minutes. Mac1+ cells were sorted using LS columns (Miltenyi, Cat#130-042-
777 401) and incubated with Mac1-PE and Ly6g-APC for 20 minutes. Mac1+ Ly6g- (monocytes) and
778 Mac1+ Ly6g+ cells (granulocytes) were sorted using either FACS Aria or Influx cell sorters.

779 For granulocyte-monocyte progenitors (GMPs), bone marrow-derived cells were lineage-
780 depleted using a Lineage Cell Depletion Kit (Miltenyi, Cat#130-090-858). Lineage negative cells
781 were then incubated with Cd34-APC, cKit-APC-Cy7, Sca1-PE-Cy7 and Cd16/32-FITC for 1.5
782 hours. Sca1- cKit+ Cd34+ Cd16/32+ cells (GMPs) were sorted using either FACS Aria or Influx
783 cell sorters.

784 For 3T3 NIH fibroblasts cells infected with C/EBP α -ER-IRES-hCD4 (WT and T35A) were
785 incubated with 0.1 μ g per 1 million cells of both Fc block and hCD4-Biotin antibody (BD
786 Pharmingen, Cat#555347) for 10 and 20 minutes respectively, followed by 10 μ L of magnetic
787 streptavidin beads (Miltenyi, Cat#130-048-101) for an additional 20 minutes. hCD4+ cells were
788 purified using LS columns (Miltenyi, Cat#130-042-401).

789 For B lymphoblastic leukemia cells (RCH-ACV) cells stably infected with C/EBP α -ERT2-
790 IRES-GFP, rtTA-Puro and TetO-Carm1-IRES-TdTomato were induced with 1 μ g/ml of
791 doxycycline (Sigma-Aldrich, Cat#D9891). GFP+ and TdTomato+ cells were single cell-sorted
792 using either FACS Aria or Influx cell sorters.

793 In co-cultures between B cells and feeder cells, non-adherent cells were collected, and joined
794 with trypsinized adherent cells centrifuged at 300 RCF for 5 minutes. Cells were re-suspended
795 in 100 μ L PBS containing 1 μ g/mL of mouse Fc block for 10 minutes. Conjugated primary
796 antibodies were added to the blocking solution and cells were further incubated at 4°C in the
797 dark for 20 minutes. Cells were washed with additional 1mL of PBS and centrifuged at 300 rcf
798 for 5 minutes. The supernatant was discarded and cells were re-suspended in 500 μ L of PBS
799 containing 5 μ g/mL of DAPI. Samples were processed in a FACS analyzer (LSR II, BD; Fortessa,
800 BD) with DiVa software and data analyzed using FlowJo software.

801 Antibodies used for cell sorting and flow cytometry are listed in **Table S1**.

802 **Phagocytosis assay**

803 After B cell to macrophage transdifferentiation, cells were removed from feeder cells through
804 differential adherence to tissue culture dishes for 40 minutes. Around 200,000 of the resulting B
805 cells (or induced macrophages) were plated in each well of a 24-well plate containing 0.01%
806 poly-L-lysine-treated coverslips (Corning, Cat#354085) in 10% FBS-DMEM supplemented with
807 IL-3 (Peprotech, Cat#213-13), mCSF-1 (Peprotech, Cat#315-03B) and cultured at 37°C
808 overnight in the presence of 1:1000 diluted blue fluorescent carboxylated microspheres
809 (Fluoresbrite, Cat#17458-10). Cells were centrifuged at 1000 RCF for 5 minutes to improve
810 attachment to the coverslips. The supernatant was removed and the cells were washed once
811 with PBS.

812 For fixation, 4% PFA was added to the wells for 20 minutes, cells were washed twice with
813 PBS and cell membranes permeabilized with 0.1% Triton X-100 PBS (0.1% PBST) for 15

814 minutes at room temperature. Cells were blocked using 0.1% PBST with 3% Bovine Serum
815 Albumin (BSA) for 30-45 minutes. Cells were washed twice in PBS. Actin filaments were
816 subsequently stained with 1:100 diluted red phalloidin (Alexa Fluor 568, Thermo Fisher Scientific,
817 Cat#A12380) while DNA was stained with a 1:500 diluted yellow probe (Quant-iT PicoGreen
818 dsDNA Assay Kit, Thermo Fischer Scientific, Cat#P7589). Cells were incubated with the two
819 dyes in 0.1% PBST containing 1% BSA at room temperature for 1 hour in the dark and washed
820 twice with PBS afterwards. Coverslips carrying the attached cells in the well were then recovered
821 with tweezers and mounted upside-down onto a charged glass slide containing a 14 μ L drop of
822 mounting medium (7 μ L Dako + 7 μ L 0.1% PBST). Coverslips were sealed with nail polish and
823 imaged in a Leica TCS SPE inverted confocal microscope.

824 Antibodies used for immunofluorescence and intracellular staining for flow cytometry are
825 listed in **Table S2**.

826 **Proximity ligation assay (PLA)**

827 Proximity ligation assay was performed using Duolink Orange Kit (Sigma-Aldrich,
828 Cat#DUO92007). Briefly, after sorting or culturing desired cell populations, 8.000 – 100.000 cells
829 per well were seeded into 24-well plates containing 0.01% poly-L-lysine (Sigma) treated
830 coverslips in appropriate medium, centrifuged at 1000 x g for 5 minutes and fixed with 4% PFA
831 for 15 minutes. Subsequent steps were performed according to the kit's protocol with antibody
832 concentrations identical to those used for immunofluorescence. Coverslips were mounted using
833 Fluoroshield mounting medium with DAPI (Abcam, Cat#ab104139) and imaged in a Leica TCS
834 SPE confocal microscope.

835 **Intracellular staining for flow cytometry**

836 After antibody staining of cell surface markers, cells were fixed in 4% BSA for 10 minutes at room
837 temperature in a rotating wheel. Fixation was stopped with two washes in PBS. Cells were
838 permeabilized in 0.1% PBST at room temperature in a rotating wheel for 10 minutes. Cells were
839 blocked using 0.1% PBST with 3% Bovine Serum Albumin (BSA) for 30-45 minutes. Cells were
840 washed twice in PBS. Cells were incubated with primary antibodies and secondary antibodies
841 diluted at the stated concentrations in 0.1% PBST with 1% BSA for 2 and 1 hours, respectively,
842 with two washes in PBS in between and after. Cells were resuspended in PBS and processed in

843 a FACS analyzer (LSR II, BD; Fortessa, BD) with DiVa software and data analyzed using FlowJo
844 software.

845 Antibodies used for immunofluorescence and intracellular staining for flow cytometry are
846 listed in **Table S2**.

847 **Protein extraction, immunoprecipitation and Western blotting**

848 Preparation of whole cell lysates and immunoprecipitation of WT or mutant C/EBP α proteins
849 were performed as previously described (Kowenz-Leutz et al., 2010). Briefly, cells were lysed
850 (20 mM HEPES pH 7.8, 150 mM NaCl, 1 mM EDTA pH 8, 10 mM MgCl₂, 0,1% Triton X-100,
851 10% Glycerol, protease inhibitor cocktail (Merck), 1mM DTT, 1mM PEFA bloc (Böhringer).
852 Immunoprecipitation was performed with appropriate antibodies as indicated for 2 h at 4°C.
853 Immunoprecipitated proteins were collected on Protein A Dynabeads (Invitrogen, Cat#100001D)
854 or Protein-G Dynabeads (Invitrogen, Cat#10004D), separated by SDS-PAGE (Mini PROTEAN
855 TGX, 4-15%, Bio-RAD #5671084). For Western blotting, samples were loaded in 10% Mini-
856 PROTEAN TGX gels (Bio- Rad) and resolved by electrophoresis in running buffer (**Table S3**).
857 Protein samples were transferred to a methanol pre-activated PVDF membrane (Bio-Rad,
858 Cat#1620177, Bio-Rad) by running them in transfer buffer (TBS) (**Table S3**) for 1 hour at 300mA
859 and 4°C. Membranes were rinsed in milliQ water and protein transfer was checked by Ponceau
860 staining (Sigma). Transferred membranes were washed once with TBS and three times with
861 TBS- Tween (TBST) (**Table S3**) followed by 5% milk in TBST for 45 min. Membranes were then
862 incubated with primary antibodies (**Table S4**) in 5% milk TBST, rotating overnight at 4°C, then
863 washed three times with TBST followed by incubation with the secondary antibodies conjugated
864 to horseradish peroxidase in 5% milk TBST for 1 hour. After three TBST washes, proteins were
865 detected using enhanced chemiluminescence reagents (Amersham ECL Prime Western Blotting
866 detection) in an Amersham Imager 600 analyzer or visualized by ECL (GE Healthcare, UK)..
867 Quantification of band intensity from scanned blots was performed with Fiji software.

868 **Electrophoretic mobility shift assay**

869 Nuclear extracts were prepared from transfected HEKT cells by a mininuclear extract protocol
870 (Schreiber et al., 1989). Electrophoretic mobility shift assays (EMSA) was performed as
871 previously described (Kowenz-Leutz et al., 1994) using double stranded IRDye Oligonucleotides
872 containing a C/EBP-binding site: IRD800-GACACTGGATTGCGCAATAGGCTC and IRD800-

873 GAGCCTATTGCGCAATCCAGTGTC (Metabion). Briefly, binding reactions with nuclear extracts
874 (2,5µg) and double stranded IRD800 oligos (20pmol) were incubated for 15 min on ice, orange
875 loading dye (Li-Cor, Cat# P/N 927-10100) was added and protein-DNA complexes were
876 separated on a 5% native polyacrylamide gel in 0,5x TBE at 25mA at room temperature. EMSA
877 results were visualized and quantified (Odyssey scanner, Licor, channel 800nm).

878 ***In vitro* protein methylation assay**

879 Methylation of peptides (PSL, Heidelberg, Germany, **Table S5**) was performed using the
880 bioluminescence-based MTase-Glo™ Assay (Promega, Cat#V7601) according to the
881 manufacturer's protocol. Assay conditions: 200 ng of enzyme was incubated with 5µM Peptide,
882 10 µM S-adenosyl-L-(methyl)-methionine as methyl donor (SAM) and 6x Methyltransferase-Glo
883 reagent at 23°C for 60 minutes. S-adenosylhomocystein (SAH) generated during the reaction
884 was converted to ADP as a proportional reaction product dependent of substrate methylation by
885 the enzymes. Subsequent incubation with the Methyltransferase-Glo Detection Solution at 23°C
886 for 30 minutes converts ADP to ATP that is used in a luciferase/luciferin-based reaction and
887 determined as relative light units (RLU) in a Berthold luminometer (Hsiao et al., 2016).

888 **RNA sequencing**

889 RNA was extracted with a miRNeasy mini kit (217004, Qiagen), quantified with a NanoDrop
890 spectrophotometer and its quality examined in a fragment Bioanalyzer (Aligent 2100 Bioanalyzer
891 DNA 7500 assay). cDNA was synthesized with a High-Capacity RNA-to-cDNA kit (4387406,
892 Applied Biosystems). For RNA-sequencing (RNA-seq), libraries were prepared with a TruSeq
893 Stranded mRNA Library Preparation Kit (Illumina) followed by single-end sequencing (50 bp) on
894 a HiSeq2500 instrument (Illumina), obtaining at least 40 million reads per sample.

895 Quality control of FASTQ reads was performed using FastQC version v.0.11.3. Reads
896 were mapped aligned to the mm10 genome using STAR version 2.5.0a (Dobin et al., 2013).
897 Gene counts were quantified Gene expression was quantified using STAR (--quantMode
898 GeneCounts). Normalized counts and differential gene expression analysis was carried out using
899 DESeq2 version 1.14.1 (Love et al., 2014). For each transdifferentiation experiment, timepoint
900 0h was set as a reference point and any gene that exhibited a statistically significant change in
901 expression ($\log_2FC \geq 0.5849625$ and $p\text{-value} \leq 0.05$) at a later timepoint was isolated. For PCA,
902 \log_2 DESeq2 normalized counts of differentially expressed genes averaged across replicates

903 were used. The R `prcomp()` command with `scale=T` was used. Pheatmap version 1.0.12 was
904 used to visualize changes in gene expression for all the isolated differentially expressed genes
905 with the following clustering options: `clustering_distance_rows="correlation"`,
906 `clustering_method="ward.D2"`, `scale="row"`.

907 *Scatter plots*

908 Differentially expressed genes (DEGs) were determined for each timepoint as described in
909 the "Materials and Methods". The union of identified DEGs in the WT and R35A systems per
910 timepoint were used to generate scatterplots depicting the \log_2FC changes of the
911 aforementioned genes for each transdifferentiation system. A regression line, colored in red, was
912 fit for each scatterplot using the `geom_smooth(method=lm)` R command. The identity line ($y=x$
913 line) is depicted in green. The spearman correlation coefficient (`cor(method="spearman")`
914 function in R) and the number of DEGs are also depicted per scatterplot.

915 **Gene ontology analysis**

916 Functional analyses by GO were performed with the R package "g:profiler2" version 0.2.0
917 (Raudvere et al., 2019). Balloonplots depict all pathways associated with a specific keyword that
918 were found enriched in at least 1 cluster. Metaplots for each cluster depict the average \log_2FC
919 values of genes per timepoint and per cluster. Shaded background corresponds to the mean
920 values ± 1.644854 standard deviation. Gene expression analysis of signature genes was
921 performed using the individual values of genes listed in **Table S6** and normalized to timepoints
922 0h for B cell genes and 120h for macrophage genes.

923 **Chromatin accessibility by ATAC-seq**

924 ATAC-seq was performed as published (Buenrostro et al., 2015). Briefly, cells were harvested
925 at the mentioned timepoints, feeder-depleted and lysed and 50.000 cells used per condition.
926 Immediately, transposition was performed using Nextera Tn5 Transposase (15027865, Illumina)
927 at 37°C for 30 minutes. Chromatin was then purified using Qiagen MinElute PCR Purification Kit
928 (28004, Qiagen). DNA was then amplified using NEBNext High Fidelity PCR Master Mix
929 (M0541S, New England Biolabs Inc.) and barcoded primers (see table MMX). qPCR was
930 performed to determine the optimal number of cycles for each condition to stop amplification prior
931 to saturation. Quality was analyzed by gel electrophoresis and in a fragment Bioanalyzer (Agilent
932 2100 Bioanalyzer DNA 7500 assay).

933 Read quality was assessed with FastQC version v.0.11.3. Adaptors were removed using
934 Cutadapt (version 0.4.2_dev) TrimGalore! In paired end mode (--paired --nextera)(Martin,
935 2011). Reads were aligned to the mm10 genome using bowtie2 (v 2.2.4) in paired end mode with
936 standard parameters. Output SAM files were converted to BAM files using samtools (v 0.1.19)
937 (Li et al., 2009). BAM files were sorted and indexed using the samtools commands sort and index,
938 respectively. Low quality reads and reads associated with a not primary or supplementary
939 alignment SAM flag were filtered out using the samtools command "samtools view -F 2304 -b -q
940 10". PCR duplicates were removed with Picard MarkDuplicates (version 2.3.0) with the following
941 options: "REMOVE_DUPLICATES=true ASSUME_SORTED=true VERBOSITY=WARNING".

942 Filtered BAM files were indexed with samtools index and were used as input in the
943 bamCoverage command of deeptools (v3.0.1)(Ramírez et al., 2014) in order to generate bigwig
944 files. bamCoverage was used with the options --binSize 1 --normalizeUsing RPGC --
945 effectiveGenomeSize 2150570000 --extendReads --outFileFormat bigwig. In order to call peaks,
946 bam files of each timepoint and experiment were merged using the samtools merge command.
947 Resulting merged bam files were indexed, and peaks were called using MACS2 with the options
948 -f BAMPE --nolambda --nomodel -g mm -q 0.05.

949 **Determination of differentially accessible ATAC peaks**

950 In order to pinpoint regions of interest, peaks of all timepoints and all experiments were merged
951 using the bedtools suite command bedtools merge. Read counts falling within the merged peak
952 regions were calculated using the Rsubread package and the featurecounts command with the
953 options isPairedEnd=T, strandSpecific=0, useMetaFeatures=F. For each transdifferentiation
954 experiment, DESeq2 was used in order to compare all timepoints with timepoint 0h. Any peak
955 showing a $\log_{2}FC \geq 1$ & Adjusted p-value ≤ 0.05 & average counts across timepoints ≥ 5 was
956 termed as a differentially accessible region and was kept for further analyses. The total number
957 of peaks isolated was 91830. Variance stabilized counts were calculated for the isolated regions
958 using the DESeq2 command varianceStabilizingTransformation and the options "blind=T",
959 fitType="parametric". Variance stabilized counts were averaged across timepoint replicates by
960 raising them at the power of 2, extracting their average and log2 transforming the resulting mean.
961 PCA was applied to this dataset using the R prcomp command, with "scale=T".

962 To group peaks, PCA was initially applied and PC1 and PC2 values for the 91,830 regions
963 were used in order to arbitrary cluster peaks into 3 groups depending on the sign of their PC1
964 and PC2 values. Values for each of the 3 groups were visualized using the pheatmap package.
965 Visual examination of the 3 main groups showed different trends: Peaks whose accessibility is
966 higher at 120h (43429 peaks), is lower at 120h (36380 peaks) and is higher at 18h (12021 peaks).

967 **Motif analysis**

968 Peaks from the 3 different groups were centered and extended 50bp upstream and downstream.
969 Nucleotide sequences for each centered peak were extracted using bedtools getfasta.
970 Sequences were submitted into MEME-ChIP with the following parameters: -dna -seed 49 -
971 meme-nmotifs 20 -meme-minw 5 -meme-minsites 2 -meme-minw 4 -meme-maxw 12. TOMTOM
972 was run using the output meme.txt file in order to identify matches of known transcription factor
973 motifs to the *de novo* discovered motifs. For each TOMTOM output a series of additional filtering
974 steps were undertaken:

- 975 1. *De novo* motif sequences need to have $\leq 75\%$ rate for each nucleotide (filtering out
976 repetitive motifs).
- 977 2. TOMTOM q-values have to be ≤ 0.01 .
- 978 3. The matched transcription factor has to be expressed at least at one timepoint.

979 **Promoter accessibility analysis**

980 Genomic coordinates of mm10 genes were downloaded from the UCSC table browser (RefSeq
981 genes). A single promoter region was assigned to each gene. The region consisted of 1kb
982 upstream and downstream of the transcription start site of the largest transcript of each gene.
983 Counts for each timepoint and each transdifferentiation experiment were assigned to each
984 promoter as described above. DESeq2 was used in order to identify differentially accessible
985 promoters as described above with the following differences regarding the cutoffs used:
986 $\text{FoldChange} \geq 1.5$ & $p\text{-value} \leq 0.05$. Variance stabilized counts were extracted for each
987 differentially accessible promoter, a mean value per replicate was extracted and the values were
988 plotted using pheatmap. Promoters were then grouped into 8 clusters. Balloonplots depict all
989 pathways associated with a specific keyword that were found enriched in at least 1 cluster.

990 For each promoter cluster and each promoter, log₂FC changes were extracted by comparing
991 expression levels (DESeq2 normalized counts) of every timepoint with the corresponding
992 timepoint 0h of the experiment.

993 **Virtual ChIP**

994 C/EBP α and PU.1 binding profiles from ChIP-seq experiments in mouse B cell to macrophage
995 transdifferentiation system were retrieved from earlier work (Van Oevelen et al., 2015). C/EBP α
996 and PU.1 peaks from timepoints 0h, 3h, 12h and 24h were pooled and merged using the bedtools
997 merge command. Each peak was assigned a unique identifier corresponding to the timepoints
998 and experiments the peak was “present”. 6 different groups of peaks were extracted from the
999 pooled file:

1000 1, 2 and 3._Peaks bound by PU.1 at 0h but not at 24h. Group was split further into two sub-
1001 groups depending on whether C/EBP α was found to bind at any timepoint.

1002 4, 5 and 6._Peaks bound by C/EBP α at 24h but not at 0h. Group was split further into two
1003 sub-groups depending on whether PU.1 was found to bind at any timepoint.

1004 Three different kinds of plots were used to summarize the accessibility dynamics of the six
1005 group of peaks in our transdifferentiation system. For each peak the average ATAC-seq bigwig
1006 score was calculated using deeptools multiBigwigSummary. Any peak overlapping with mm10
1007 encode blacklisted regions was excluded. Values were averaged across timepoint replicates and
1008 visualized in R using the pheatmap package. The same values used for the heatmap peak values
1009 were used. Z-transformed values were calculated for every peak.

1010 **Single molecule tracking (SMT)**

1011 30,000 NIH 3T3 cells inducible for CEBPAwt-HALO or CEBPAr35a-HALO were seeded in a
1012 LabTek-II chambered 8 well plates (Lab-Tek 155049), and induced for 6h or 24h with 1ug/ml
1013 doxycycline, with or without prior infection with TETO-FUW-PU.1 lentivirus infection. Right before
1014 imaging, cells were treated with 5nM of Janelia Fluor 549 (JF549) HaloTag ligand (a kind gift
1015 from Luke Lavis, HHMI) for 15 minutes. Cells were subsequently washed three times in PBS at
1016 37C, and Phenol Red-free High Glucose medium was added to each well. All imaging was
1017 carried out under HILO conditions (Tokunaga et al., 2008). For imaging experiments, one frame
1018 was acquired with 100ms of exposure time (10 Hz) to measure the intensity of fluorescence of

1019 the nuclei, and in SMT)experiments, 5000 frames were acquired with an exposure of 10ms (100
1020 Hz).

1021 Imaging experiments were carried out in Phenol red-free High Glucose Medium
1022 (ThermoFisher, Cat#21063029) pyruvate, GlutaMAX, in an imaging chamber heated at 37°C
1023 (more details in the Single Molecule Live Cell Imaging section). All live-cell imaging experiments
1024 of SMT were carried out in a Nanoimager S from Oxford Nanoimaging Limited (ONI), in a
1025 temperature and humidity-controlled chamber, a scientific Complementary metal–oxide–
1026 semiconductor (sCMOS) camera with a 2.3 electrons rms read noise at standard scan, a 100X,
1027 1.49 NA oil immersion objective and a 561 nm green laser. Images were acquired with the
1028 Nanoimager software. Quantification and Statistical Analysis of SMT was performed as
1029 previously described (Lerner et al., 2020). All scripts are publicly available.

1030 **Two Parameter SMT Tracking Analysis**

1031 In brief, TIF stacks SMT movies were analyzed using MATLAB-based SLIMfast script (Teves et
1032 al., 2016) a modified version of MTT (Sergé et al., 2008), with a Maximal expected Diffusion
1033 Coefficient (DMax) of 3 $\mu\text{m}^2/\text{s}$. The SLIMfast output .txt files were reorganized by the
1034 homemade csv_converter.m MATLAB script (available in (Lerner et al., 2020) in .csv format for
1035 further analysis. The single molecule tracking .csv files (see previous section) were first classified
1036 by the homemade SMT_Motion_Classifier.m MATLAB script. Single molecule trajectories (or
1037 tracks) with a track duration shorter than 5 frames were discarded from the analysis. Motion
1038 tracks are classified by the script in different groups: tracks with $\alpha \leq 0.7$ were considered as
1039 Confined; motion tracks with $0.7 < \alpha < 1$ as Brownian; and motion tracks with $\alpha \geq 1$ as Directed.
1040 In addition, the motion tracks showing a behavior similar to a levy-flight (presenting mixed
1041 Confined and Directed/Brownian behavior) were detected by the presence of a jump superior to
1042 the average jump among the track + a jump threshold of 1.5, and classified as “Butterfly.” Butterfly
1043 motion tracks were segmented into their corresponding Confined and Directed/Brownian sub-
1044 trajectories for posterior analysis. As an additional filtering step of confined motions (including
1045 confined segments of Butterfly tracks), we defined a jump threshold of 100nm, to filter out motion
1046 tracks with an average frame-to-frame jump size larger than 100nm.

1047 **Data mining of published datasets**

1048 DNA-binding peaks of C/EBP α and PU.1 during BMT were extracted from (Van Oevelen et al.
1049 2015) and analysed as stated above. Single-cell expression trajectories and correlations in B cell
1050 transdifferentiation and reprogramming were processed from (Francesconi et al., 2019). Gene
1051 expression data from hematopoietic cells (CMP, GMP, Monocyte and Granulocyte (neutrophil))
1052 were from (Ohlsson et al., 2016).

1053 **Statistical analyses**

1054 Statistical analyses were performed using Prism 9 software. To calculate significance, samples
1055 from at least 3 biologically independent experiments were analyzed. Two biological replicates
1056 were used for RNA- and ATAC- sequencing experiments and statistics applied to the expression
1057 of a collection of genes. For samples with $n \geq 3$, values shown in the figures represent mean \pm
1058 standard deviation. Box plots represent median with quartiles and whiskers and individual values
1059 are shown. One-way, two-way ANOVA (with the corresponding multiple comparison analyses)
1060 and Student's t-tests were applied accordingly. P-values appear indicated in each figure only
1061 when ≤ 0.05 . In time-course experiments, p-values of differences between conditions by two-
1062 way ANOVA are shown. In box plots, p-values of each individual timepoint as well as p-values
1063 of differences between conditions by two-way ANOVA are shown.

1064

1065 **Table S1. List of antibodies used for cell sorting and Flow cytometry experiments**

FACS/Cell sorting				
Antibody	Company	Catalogue	Species	Dilution
Cd16/Cd32 (FcBlock)	BD Pharmingen	553142	Rat	1:400
Cd19-Biotin	BD Biosciences	553784	Rat	1:400
Mac1-Biotin	BD Pharmingen	557395	Rat	1:400
hCD4-Biotin	eBioscience	13-0049	Mouse	1:33
Cd19-APC	BD Pharmingen	550992	Rat	1:400
Mac1-PE-Cy7	BD Pharmingen	552850	Rat	1:400
Ly6g-PE	Pharmingen	553128	Rat	1:400

Mac1-APC	eBioscience	17-0112-83	Rat	1:400
hCD4-PE	BD Pharmingen	555347	Mouse	1:20
hCD16/CD32 (hFcBlock)	Invitrogen	16-9161-73	-	1:20
hCD19-APC-Cy7	BD Pharmingen	557791	Mouse	1:33
hMac1-APC	BD Pharmingen	561015	Mouse	1:33
Cd16/Cd32-FITC	BD Pharmingen	553144	Rat	1:400
cKit-APC-Cy7	Invitrogen	47-1172-82	Rat	1:400
Cd34-APC	BD Pharmingen	560230	Rat	1:50
Sca1-PE-Cy7	BD Pharmingen	558162	Rat	1:400
Sca1-PerCP-Cy5.5	eBioscience	35-5981-82	Rat	1:400
Cd41-PE-Cy7	eBioscience	25-0411-82	Rat	1:400

1066

1067 **Table S2. List of antibodies and fluorochromes used for immunofluorescence and**
 1068 **intracellular staining for flow cytometry**

Intracellular staining for flow cytometry				
Antibody	Company	Catalogue	Species	Dilution
C/EBP α	Cell Signaling	8178	Rabbit	1:100
Carm1	Cell Signaling	12495	Mouse	1:100
PU.1	Abcam	Ab88082	Mouse	1:100
BAFF155	Cell Signaling	D7F8S	Rabbit	1:200
BAFF155- AsDM	Cell Signaling	94962	Rabbit	1:200
AF488 Anti- rabbit	ThermoFisher	A-11070	Goat	1:500

AF555 Anti-mouse	ThermoFisher	A-21422	Goat	1:500
------------------	--------------	---------	------	-------

1069

1070 **Table S3. Chemical reagents used to prepare buffers for western blot.**

Running buffer	Transfer buffer	TBST
25mM Tris-base	25mM Tris-HCl pH=3.8	10mM Tris HCl=7.5
200mM glycine	200mM glycine	100mM NaCl
0.1% SDS	20% methanol	0.1% Tween 20

1071 **Table S4. List of antibodies used for western blot experiments**

Antibody	Company	Catalogue	Species	Dilution
C/EBP α	Cell Signaling	8178	Rabbit	1:1000
aDMA	Cell Signaling	13522S	Rabbit	1:1000
aDMA	Upstate	#07-414	Rabbit	1:1000
HA	Covance	#MMS-101R	Mouse	1:1000
Flag	Sigma	F3165	Mouse	1:1000
Flag	Abnova	PAB 29056	Chicken	1:1000
BAFF155	Cell Signaling	D7F8S	Rabbit	1:1000
BAFF155-AsDM	Cell Signaling	94962	Rabbit	1:1000
PU.1	Abcam	Ab88082	Mouse	1:1000
Vinculin	Merck	V9131	Mouse	1:200

Gapdh	Abcam	Ab8245	Mouse	1:5000
H3	Abcam	Ab10799	Mouse	1:1000

1072

1073 **Table S5. List of peptides used for in vitro methylation experiments**

Peptides
YEAEP R PPMSS, aa 7-17
AFGF P R G AGPA, aa 30-40
LFQHS R QQEKA, aa 81-91
GYLD G R L EPLY, aa 137-147
EPLYE R VGAPA, aa 144-154
GAPAL R PLVIK, aa 151-161
IKQEP R EEDEA, aa 160-170
AHPDL R ASGGS, aa 259-269
SNEY R V R R R ERNNIA, aa 282-295
NIAV R K S R D KAK, aa 293-304
DKAK Q R N VETQ, aa 301-311
SDND R L R K R VEQL, aa 319-331
VEQL S R E LDTL, aa 328-338
ELDTL R G I F R QLPES, aa 334-348
MSSHLQSPPHAPSSAAFG F P R GAGP AQPPAPPA A PEPLGG aa 15-54

MSSHLQSPPHAPSSAAF G F P R(me2) GAGPAQPPAPPAAPEPLGG aa 15- 54
MSSHLQSPPHAPSSAAF G F P R/AGA GPAQPPAPPAAPEPLGG aa 15-54
PRMT4 peptide substrate
Histone H3 aa 1-21
Histone H4 aa 1-21

1074

1075 **Table S6. List of genes used to analyze kinetics of specific signatures**

B cell genes – Figure S1H
<i>Pax5, Ebf1, Foxo1, Ikzf1, Rag1, Rag2, Bcl11a, Spib, Ikzf3, Cd2, Cd19, Igl1, Vpreb1, Vpreb2, Vpreb3, Pou2a1, Blk, Cd79a, Cd79b, Lef1</i>
Macrophage genes – Figure S1H
<i>C1qc, Fcer1g, Sell, Ccr1, Mitf, Tlr2, Csf1r, Trem2, Fam20c, Adam8, Batf2, Fes, Itgam, Ccl3, Cd300lf, Tnsf9, Tyrobp, Cd14, Ifitm6, Csf3r</i>

1076

1077 **Newly Created Materials**

1078 The new constructs and cell lines listed can be requested from the corresponding authors. The
1079 sequencing data will be deposited at GEO and made freely available

1080 **Competing interests**

1081 The authors declare no competing interests

1082 **REFERENCES**

- 1083 Arinobu Y, Mizuno S, Chong Y, Shigematsu H, Iino T, Iwasaki H, Graf T, Mayfield R, Chan S,
1084 Kastner P, Akashi K. 2007. Reciprocal Activation of GATA-1 and PU.1 Marks Initial
1085 Specification of Hematopoietic Stem Cells into Myeloerythroid and Myelolymphoid Lineages.
1086 *Cell Stem Cell* **1**:416–427. doi:10.1016/j.stem.2007.07.004
- 1087 Bedford MT, Clarke SG. 2009. Protein Arginine Methylation in Mammals: Who, What, and Why.
1088 *Mol Cell* **33**:1–13. doi:10.1016/j.molcel.2008.12.013
- 1089 Bedford MT, Richard S. 2005. Arginine methylation: An emerging regulator of protein function.
1090 *Mol Cell* **18**:263–272. doi:10.1016/j.molcel.2005.04.003
- 1091 Buenrostro JD, Wu B, Chang HY, Greenleaf WJ. 2015. ATAC-seq: A method for assaying
1092 chromatin accessibility genome-wide. *Curr Protoc Mol Biol* **2015**:21.29.1-21.29.9.
1093 doi:10.1002/0471142727.mb2129s109
- 1094 Bussmann LH, Schubert A, Vu Manh TP, De Andres L, Desbordes SC, Parra M, Zimmermann
1095 T, Rapino F, Rodriguez-Ubrea J, Ballestar E, Graf T. 2009. A Robust and Highly Efficient
1096 Immune Cell Reprogramming System. *Cell Stem Cell* **5**:554–566.
1097 doi:10.1016/j.stem.2009.10.004
- 1098 Cai DH, Wang D, Keefer J, Yeaman C, Hensley K, Friedman AD. 2008. C/EBP α :AP-1 leucine
1099 zipper heterodimers bind novel DNA elements, activate the PU.1 promoter and direct
1100 monocyte lineage commitment more potently than C/EBP α homodimers or AP-1. *Oncogene*
1101 **27**:2772–2779. doi:10.1038/SJ.ONC.1210940
- 1102 Chang NC, Sincennes MC, Chevalier FP, Brun CE, Lacaria M, Segalés J, Muñoz-Cánoves P,
1103 Ming H, Rudnicki MA. 2018. The Dystrophin Glycoprotein Complex Regulates the
1104 Epigenetic Activation of Muscle Stem Cell Commitment. *Cell Stem Cell* **22**:755-768.e6.
1105 doi:10.1016/j.stem.2018.03.022
- 1106 Chen J, Zhang Z, Li L, Chen BC, Revyakin A, Hajj B, Legant W, Dahan M, Lionnet T, Betzig E,
1107 Tjian R, Liu Z. 2014. Single-molecule dynamics of enhanceosome assembly in embryonic
1108 stem cells. *Cell* **156**:1274–1285. doi:10.1016/j.cell.2014.01.062
- 1109 Choi J, Baldwin TM, Wong M, Bolden JE, Fairfax KA, Lucas EC, Cole R, Biben C, Morgan C,
1110 Ramsay KA, Ng AP, Kauppi M, Corcoran LM, Shi W, Wilson N, Wilson MJ, Alexander WS,
1111 Hilton DJ, De Graaf CA. 2019. Haemopedia RNA-seq: A database of gene expression during
1112 haematopoiesis in mice and humans. *Nucleic Acids Res* **47**:D780–D785.
1113 doi:10.1093/nar/gky1020
- 1114 Deribe YL, Pawson T, Dikic I. 2010. Post-translational modifications in signal integration. *Nat*
1115 *Struct Mol Biol* **17**:666–672. doi:10.1038/nsmb.1842
- 1116 Di Stefano B, Sardina JL, Van Oevelen C, Collombet S, Kallin EM, Vicent GP, Lu J, Thieffry D,
1117 Beato M, Graf T. 2014. C/EBP α poises B cells for rapid reprogramming into induced
1118 pluripotent stem cells. *Nature* **506**:235–239. doi:10.1038/nature12885
- 1119 Dobin A, Davis CA, Schlesinger F, Drenkow J, Zaleski C, Jha S, Batut P, Chaisson M, Gingeras
1120 TR. 2013. STAR: Ultrafast universal RNA-seq aligner. *Bioinformatics* **29**:15–21.
1121 doi:10.1093/bioinformatics/bts635
- 1122 Ebisuya M, Briscoe J. 2018. What does time mean in development? *Development* **145**.
1123 doi:10.1242/dev.164368

- 1124 Eyquem S, Chemin K, Fasseu M, Chopin M, Sigaux F, Cumano A, Bories JC. 2004. The
1125 development of early and mature B cells is impaired in mice deficient for the Ets-1
1126 transcription factor. *Eur J Immunol* **34**:3187–3196. doi:10.1002/EJL.200425352
- 1127 Feng R, Desbordes SC, Xie H, Tillo ES, Pixley F, Stanley ER, Graf T. 2008. PU.1 and C/EBP α / β
1128 convert fibroblasts into macrophage-like cells. *Proceedings of the National Academy of*
1129 *Sciences* **105**:6057–6062. doi:10.1073/pnas.0711961105
- 1130 Fernandez Garcia M, Moore CD, Schulz KN, Alberto O, Donague G, Harrison MM, Zhu H, Zaret
1131 KS. 2019. Structural Features of Transcription Factors Associating with Nucleosome
1132 Binding. *Mol Cell* **75**:921-932.e6. doi:10.1016/j.molcel.2019.06.009
- 1133 Francesconi M, di Stefano B, Berenguer C, Andrés-Aguayo L de, Plana-Carmona M, Mendez-
1134 Lago M, Guillaumet-Adkins A, Rodriguez-Esteban G, Gut M, Gut IG, Heyn H, Lehner B, Graf
1135 T. 2019. Single cell RNA-seq identifies the origins of heterogeneity in efficient cell
1136 transdifferentiation and reprogramming. *Elife* **8**:1–22. doi:10.7554/eLife.41627
- 1137 Graf T, Enver T. 2009. Forcing cells to change lineages. *Nature* **462**:587–594.
1138 doi:10.1038/nature08533
- 1139 Greenblatt SM, Man N, Hamard PJ, Asai T, Karl D, Martinez C, Bilbao D, Stathais V, McGrew-
1140 Jermacowicz A, Duffort S, Tadi M, Blumenthal E, Newman S, Vu L, Xu Y, Liu F, Schurer
1141 SC, McCabe MT, Kruger RG, Xu M, Yang FC, Tenen D, Watts J, Vega F, Nimer SD. 2018.
1142 CARM1 Is Essential for Myeloid Leukemogenesis but Dispensable for Normal
1143 Hematopoiesis. *Cancer Cell* **33**:1111-1127.e5. doi:10.1016/j.ccell.2018.05.007
- 1144 Guo Z, Zheng L, Xu H, Dai H, Zhou M, Pascua MR, Chen QM, Shen B. 2010. Methylation of
1145 FEN1 suppresses nearby phosphorylation and facilitates PCNA binding. *Nat Chem Biol*
1146 **6**:766–773. doi:10.1038/NCHEMBIO.422
- 1147 Heath V, Suh HC, Holman M, Renn K, Gooya JM, Parkin S, Klarmann KD, Ortiz M, Johnson P,
1148 Keller J. 2004. C/EBP α deficiency results in hyperproliferation of hematopoietic progenitor
1149 cells and disrupts macrophage development in vitro and in vivo. *Blood* **104**:1639–1647.
1150 doi:10.1182/blood-2003-11-3963
- 1151 Heinz S, Benner C, Spann N, Bertolino E, Lin YC, Laslo P, Cheng JX, Murre C, Singh H, Glass
1152 CK. 2010. Simple Combinations of Lineage-Determining Transcription Factors Prime cis-
1153 Regulatory Elements Required for Macrophage and B Cell Identities. *Mol Cell* **38**:576–589.
1154 doi:10.1016/j.molcel.2010.05.004
- 1155 Hertweck A, Mucha MV De, Barber PR, Dagil R, Porter H, Ramos A, Lord GM, Jenner RG. 2022.
1156 The TH1 cell lineage-determining transcription factor T-bet suppresses TH2 gene
1157 expression by redistributing GATA3 away from TH2 genes. *Nucleic Acids Res* **1**.
1158 doi:<https://doi.org/10.1093/nar/gkac258>
- 1159 Hosokawa H, Ungerbäck J, Wang X, Matsumoto M, Nakayama KI, Cohen SM, Tanaka T,
1160 Rothenberg E V. 2018. Transcription Factor PU.1 Represses and Activates Gene
1161 Expression in Early T Cells by Redirecting Partner Transcription Factor Binding. *Immunity*
1162 **48**:1119-1134.e7. doi:10.1016/j.immuni.2018.04.024
- 1163 Hsiao K, Zegzouti H, Goueli SA. 2016. Methyltransferase-Glo: A universal, bioluminescent and
1164 homogenous assay for monitoring all classes of methyltransferases. *Epigenomics* **8**:321–
1165 339. doi:10.2217/EPI.15.113

- 1166 Hu C-J, Rao S, Ramirez-Bergeron DL, Garrett-Sinha LA, Gerondakis S, Clark MR, Simo MC.
1167 2001. PU.1/Spi-B Regulation of c-rel Is Essential for Mature B Cell Survival. *Immunity*
1168 **15**:545–555.
- 1169 Jack I, Seshadri R, Garson M, Michael P, Callen D, Zola H, Morley A. 1986. RCH-ACV: A
1170 lymphoblastic leukemia cell line with chromosome translocation 1;19 and trisomy 8. *Cancer*
1171 *Genet Cytogenet* **19**:261–269. doi:10.1016/0165-4608(86)90055-5
- 1172 Kawabe YI, Wang YX, McKinnell IW, Bedford MT, Rudnicki MA. 2012. Carm1 regulates Pax7
1173 transcriptional activity through MLL1/2 recruitment during asymmetric satellite stem cell
1174 divisions. *Cell Stem Cell* **11**:333–345. doi:10.1016/j.stem.2012.07.001
- 1175 Kim D, Lee J, Cheng D, Li J, Carter C, Richie E, Bedford MT. 2010. Enzymatic activity is required
1176 for the in Vivo functions of CARM1. *Journal of Biological Chemistry* **285**:1147–1152.
1177 doi:10.1074/jbc.M109.035865
- 1178 Klemm SL, Shipony Z, Greenleaf WJ. 2019. Chromatin accessibility and the regulatory
1179 epigenome. *Nature Reviews* **20**:207–220. doi:10.1038/s41576-018-0089-8
- 1180 Konstantinides N, Holguera I, Rossi AM, Escobar A, Dudragne L, Chen Y-C, Tran TN, Martínez
1181 Jaimes AM, Özel MN, Simon F, Shao Z, Tsankova NM, Fullard JF, Walldorf U, Roussos P,
1182 Desplan C. 2022. A complete temporal transcription factor series in the fly visual system.
1183 *Nature* **604**:316–322. doi:10.1038/s41586-022-04564-w
- 1184 Kowenz-Leutz E, Pless O, Dittmar G, Knoblich M, Leutz A. 2010. Crosstalk between C/EBPβ
1185 phosphorylation, arginine methylation, and SWI/SNF/Mediator implies an indexing
1186 transcription factor code. *EMBO Journal* **29**:1105–1115. doi:10.1038/emboj.2010.3
- 1187 Kowenz-Leutz E, Twamley G, Ansieau S, Leutz A. 1994. Novel mechanism of C/EBPβ (NF-M)
1188 transcriptional control: Activation through derepression. *Genes Dev* **8**:2781–2791.
1189 doi:10.1101/gad.8.22.2781
- 1190 Kueh HY, Champhekar A, Nutt SL, Elowitz MB, Rothenberg E v. 2013. Positive Feedback
1191 Between PU.1 and the Cell Cycle Controls Myeloid Differentiation. *Science (1979)* **341**:670–
1192 673. doi:10.1126/science.1240831
- 1193 Laiosa C V., Stadtfeld M, Xie H, de Andres-Aguayo L, Graf T. 2006. Reprogramming of
1194 Committed T Cell Progenitors to Macrophages and Dendritic Cells by C/EBPα and PU.1
1195 Transcription Factors. *Immunity* **25**:731–744. doi:10.1016/j.immuni.2006.09.011
- 1196 Leddin M, Perrod C, Hoogenkamp M, Ghani S, Assi S, Heinz S, Wilson NK, Follows G, Schönheit
1197 J, Vockentanz L, Mosammam AM, Chen W, Tenen DG, Westhead DR, Göttgens B, Bonifer
1198 C, Rosenbauer F. 2011. Two distinct auto-regulatory loops operate at the PU.1 locus in B
1199 cells and myeloid cells. *Blood* **117**:2827–2838. doi:10.1182/blood-2010-08-302976
- 1200 Lerner J, Gomez-Garcia PA, McCarthy RL, Liu Z, Lakadamyali M, Zaret KS. 2020. Two-
1201 Parameter Mobility Assessments Discriminate Diverse Regulatory Factor Behaviors in
1202 Chromatin. *Mol Cell* **79**:677–688. doi:10.1016/j.molcel.2020.05.036
- 1203 Li H, Handsaker B, Wysoker A, Fennell T, Ruan J, Homer N, Marth G, Abecasis G, Durbin R.
1204 2009. The Sequence Alignment/Map format and SAMtools. *Bioinformatics* **25**:2078–2079.
1205 doi:10.1093/bioinformatics/btp352

- 1206 Li J, Zhao Z, Carter C, Ehrlich LIR, Bedford MT, Richie ER. 2013. Coactivator-Associated
1207 Arginine Methyltransferase 1 Regulates Fetal Hematopoiesis and Thymocyte Development.
1208 *The Journal of Immunology* **190**:597–604. doi:10.4049/jimmunol.1102513
- 1209 Liu Z, Tjian R. 2018. Visualizing transcription factor dynamics. *Journal of Cell Biology* **217**:1181–
1210 1191. doi:10.1083/jcb.201710038
- 1211 Love MI, Huber W, Anders S. 2014. Moderated estimation of fold change and dispersion for
1212 RNA-seq data with DESeq2. *Genome Biol* **15**:1–21. doi:10.1186/s13059-014-0550-8
- 1213 Ma O, Hong S, Guo H, Ghiaur G, Friedman AD. 2014. Granulopoiesis Requires Increased
1214 C/EBP α Compared to Monopoiesis, Correlated with Elevated Cebpa in Immature G-CSF
1215 Receptor versus M-CSF Receptor Expressing Cells. *PLoS One* **9**:e95784.
1216 doi:10.1371/journal.pone.0095784
- 1217 Martin M. 2011. Cutadapt removes adapter sequences from high-throughput sequencing reads.
1218 *EMBnet J* **17**.1
- 1219 Moris N, Pina C, Arias AM. 2016. Transition states and cell fate decisions in epigenetic
1220 landscapes. *Nat Rev Genet* **17**:693–703. doi:10.1038/nrg.2016.98
- 1221 Nakayama K, Szewczyk MM, dela Sena C, Wu H, Dong A, Zeng H, Li F, Ferreira De Freitas R,
1222 Eram MS, Schapira M, Baba Y, Kunitomo M, Cary DR, Tawada M, Ohashi A, Imaeda Y,
1223 Singh Saikatendu K, Grimshaw CE, Vedadi M, Arrowsmith CH, Barsyte-Lovejoy D, Kiba A,
1224 Tomita D, Brown PJ. 2018. TP-064, a potent and selective small molecule inhibitor of
1225 PRMT4 for multiple myeloma. *Oncotarget* **9**:18480–18493.
- 1226 Nerlov C. 2007. The C/EBP family of transcription factors: a paradigm for interaction between
1227 gene expression and proliferation control. *Trends Cell Biol* **17**:318–324.
1228 doi:10.1016/j.tcb.2007.07.004
- 1229 Notta F, Zandi S, Takayama N, Dobson S, Gan OI, Wilson G, Kaufmann KB, McLeod J, Laurenti
1230 E, Dunant CF, McPherson JD, Stein LD, Dror Y, Dick JE. 2016. Distinct routes of lineage
1231 development reshape the human blood hierarchy across ontogeny. *Science (1979)* **351**.
1232 doi:10.1126/science.aab2116
- 1233 Ohlsson E, Schuster MB, Hasemann M, Porse BT. 2016. The multifaceted functions of C/EBP α
1234 in normal and malignant haematopoiesis. *Leukemia*. doi:10.1038/leu.2015.324
- 1235 Okawa S, Saltó C, Ravichandran S, Yang S, Toledo EM, Arenas E, Del Sol A. 2018.
1236 Transcriptional synergy as an emergent property defining cell subpopulation identity enables
1237 population shift. *Nat Commun* **9**:1–10. doi:10.1038/s41467-018-05016-8
- 1238 Orkin SH, Zon LI. 2008. Hematopoiesis: An Evolving Paradigm for Stem Cell Biology. *Cell*
1239 **132**:631–644. doi:10.1016/j.cell.2008.01.025
- 1240 Ramberger E, Sapozhnikova V, Kowenz-Leutz E, Zimmermann K, Nicot N, Nazarov P v., Perez-
1241 Hernandez D, Reimer U, Mertins P, Dittmar G, Leutz A. 2021. PRISMA and BioID disclose
1242 a motifs-based interactome of the intrinsically disordered transcription factor C/EBP α .
1243 *iScience* **24**:102686. doi:10.1016/j.isci.2021.102686
- 1244 Ramírez F, Dünder F, Diehl S, Grüning BA, Manke T. 2014. DeepTools: A flexible platform for
1245 exploring deep-sequencing data. *Nucleic Acids Res* **42**:187–191. doi:10.1093/nar/gku365

- 1246 Rapino F, Robles EF, Richter-Larrea JA, Kallin EM, Martinez-Climent JA, Graf T. 2013. C/EBP α
1247 Induces Highly Efficient Macrophage Transdifferentiation of B Lymphoma and Leukemia
1248 Cell Lines and Impairs Their Tumorigenicity. *Cell Rep* **3**:1153–1163.
1249 doi:10.1016/j.celrep.2013.03.003
- 1250 Raschke WC, Baird S, Ralph P, Nakoinz I. 1978. Functional macrophage cell lines transformed
1251 by abelson leukemia virus. *Cell* **15**:261–267. doi:10.1016/0092-8674(78)90101-0
- 1252 Raudvere U, Kolberg L, Kuzmin I, Arak T, Adler P, Peterson H, Vilo J. 2019. G:Profiler: A web
1253 server for functional enrichment analysis and conversions of gene lists (2019 update).
1254 *Nucleic Acids Res* **47**:W191–W198. doi:10.1093/nar/gkz369
- 1255 Rayon T, Stamataki D, Perez-Carrasco R, Garcia-Perez L, Barrington C, Melchionda M, Exelby
1256 K, Lazaro J, Tybulewicz VLJ, Fisher EMC, Briscoe J. 2020. Species-specific pace of
1257 development is associated with differences in protein stability. *Science (1979)* **369**.
1258 doi:10.1126/science.aba7667
- 1259 Schreiber E, Matthias P, Müller MM, Schaffner W. 1989. Rapid detection of octamer binding
1260 proteins with ‘mini extracts’, prepared from a small number of cells. *Nucleic Acids Res*
1261 **17**:6419. doi:10.1093/nar/17.15.6419
- 1262 Scott EW, Simon MC, Anastasi J, Singh H. 1994. Requirement of transcription factor PU.1 in the
1263 development of multiple hematopoietic lineages. *Science (1979)* **265**:1573–1577.
1264 doi:10.1126/science.8079170
- 1265 Sergé A, Bertaux N, Rigneault H, Marguet D. 2008. Dynamic multiple-target tracing to probe
1266 spatiotemporal cartography of cell membranes. *Nature Methods* **2008** 5:8 **5**:687–694.
1267 doi:10.1038/nmeth.1233
- 1268 Singh H, Dekoter RP, Walsh JC. 1999. PU.1, a Shared Transcriptional Regulator of Lymphoid
1269 and Myeloid Cell Fates. *Cold Spring Harb Symp Quant Biol* **64**:13–20.
1270 doi:10.1101/sqb.1999.64.13
- 1271 Springer T, Galfré G, Secher DS, Milstein C. 1979. Mac-1: a macrophage differentiation antigen
1272 identified by monoclonal antibody. *Eur J Immunol* **9**:301–306. doi:10.1002/eji.1830090410
- 1273 Stoilova B, Kowenz-Leutz E, Scheller M, Leutz A. 2013. Lymphoid to Myeloid Cell Trans-
1274 Differentiation Is Determined by C/EBP β Structure and Post-Translational Modifications.
1275 *PLoS One* **8**:e65169. doi:10.1371/journal.pone.0065169
- 1276 Suresh S, Huard S, Dubois T. 2021. CARM1/PRMT4: Making Its Mark beyond Its Function as a
1277 Transcriptional Coactivator. *Trends Cell Biol* **31**:402–417. doi:10.1016/j.tcb.2020.12.010
- 1278 Teves SS, An L, Hansen AS, Xie L, Darzacq X, Tjian R. 2016. A dynamic mode of mitotic
1279 bookmarking by transcription factors. *Elife* **5**. doi:10.7554/ELIFE.22280
- 1280 Torcal Garcia G, Graf T. 2021. The transcription factor code: a beacon for histone
1281 methyltransferase docking. *Trends Cell Biol* **31**:792–800. doi:10.1016/j.tcb.2021.04.001
- 1282 Torres-Padilla ME, Parfitt DE, Kouzarides T, Zernicka-Goetz M. 2007. Histone arginine
1283 methylation regulates pluripotency in the early mouse embryo. *Nature* **445**:214–218.
1284 doi:10.1038/nature05458
- 1285 van Oevelen C, Collombet S, Vicent G, Hoogenkamp M, Lepoivre C, Badeaux A, Bussmann L,
1286 Sardina JL, Thieffry D, Beato M, Shi Y, Bonifer C, Graf T. 2015. C/EBP α Activates Pre-

- 1287 existing and de Novo Macrophage Enhancers during Induced Pre-B Cell Transdifferentiation
1288 and Myelopoiesis. *Stem Cell Reports* **5**:232–247. doi:10.1016/j.stemcr.2015.06.007
- 1289 Velten L, Haas SF, Raffel S, Blaszkiewicz S, Hennig BP, Hirche C, Lutz C, Buss EC, Boch T,
1290 Hofmann W, Ho AD, Huber W. 2017. Human haematopoietic stem cell lineage commitment
1291 is a continuous process **19**:271–281. doi:10.1038/ncb3493.Human
- 1292 Wang K, Wei G, Liu D. 2012. CD19: a biomarker for B cell development, lymphoma diagnosis
1293 and therapy. *Exp Hematol Oncol* **1**:36. doi:10.1186/2162-3619-1-36
- 1294 Wang L, Zhao Z, Meyer MB, Saha S, Yu M, Guo A, Wisinski KB, Huang W, Cai W, Pike JW,
1295 Yuan M, Ahlquist P, Xu W. 2014. CARM1 methylates chromatin remodeling factor BAF155
1296 to enhance tumor progression and metastasis. *Cancer Cell* **25**:21–36.
1297 doi:10.1016/j.ccr.2013.12.007
- 1298 Wu Q, Schapira M, Arrowsmith CH, Barsyte-Lovejoy D. 2021. Protein arginine methylation: from
1299 enigmatic functions to therapeutic targeting. *Nat Rev Drug Discov* **20**:509–530.
1300 doi:10.1038/s41573-021-00159-8
- 1301 Xie H, Ye M, Feng R, Graf T. 2004. Stepwise reprogramming of B cells into macrophages. *Cell*
1302 **117**:663–676. doi:10.1016/S0092-8674(04)00419-2
- 1303 Xue HH, Bollenbacher-Reilley J, Wu Z, Spolski R, Jing X, Zhang YC, McCoy JP, Leonard WJ.
1304 2007. The Transcription Factor GABP Is a Critical Regulator of B Lymphocyte Development.
1305 *Immunity* **26**:421–431. doi:10.1016/J.IMMUNI.2007.03.010
- 1306 Yadav N, Cheng D, Richard S, Morel M, Iyer VR, Aldaz CM, Bedford MT. 2008. CARM1
1307 promotes adipocyte differentiation by coactivating PPAR γ . *EMBO Rep* **9**:193–198.
1308 doi:10.1038/sj.embor.7401151
- 1309 Zhang P, Iwasaki-Arai J, Iwasaki H, Fenyus ML, Dayaram T, Owens BM, Shigematsu H,
1310 Levantini E, Huettner CS, Lekstrom-Himes JA, Akashi K, Tenen DG. 2004. Enhancement
1311 of hematopoietic stem cell repopulating capacity and self-renewal in the absence of the
1312 transcription factor C/EBP α . *Immunity* **21**:853–863. doi:10.1016/j.immuni.2004.11.006
- 1313 Zhang XK, Moussa O, LaRue A, Bradshaw S, Molano I, Spyropoulos DD, Gilkeson GS, Watson
1314 DK. 2008. The Transcription Factor Fli-1 Modulates Marginal Zone and Follicular B Cell
1315 Development in Mice. *The Journal of Immunology* **181**:1644–1654.
1316 doi:10.4049/JIMMUNOL.181.3.1644
- 1317